Bachelor Thesis
University of Groningen
Kapteyn Astronomical Institute

Perturbation of the Oort Cloud by Close Stellar Encounter with Gliese 710

August 5, 2019

Author: Rens Juris Tesink
Supervisors: Kateryna Frantseva and Nickolas Oberg

Abstract

Context: Our Sun is thought to have an Oort cloud, a spherically symmetric shell of roughly 10^{11} comets orbiting with semi major axes between $\sim 5 \times 10^3$ AU and 1×10^5 AU. It is thought to be possible that other stars also possess comet clouds. Gliese 710 is a star expected to have a close encounter with the Sun in 1.35 Myrs.

Aims: To simulate the comet clouds around the Sun and Gliese 710 and investigate the effect of the close encounter.

Method: Two `REBOUND` N-body simulations were used with the help of Gaia DR2 data. Simulation 1 had a total integration time of 4 Myr, a time-step of 1 yr, and 10,000 comets in each comet cloud. And Simulation 2 had a total integration time of 80,000 yr, a time-step of 0.01 yr, and 100,000 comets in each comet cloud.

Results: Simulation 2 revealed a 1.7% increase in the semi-major axis at time of closest approach and a population loss of 0.019% - 0.117% for the Oort cloud. There was no statistically significant net change of the inclination of the comets during this encounter and a 0.14% increase in the eccentricity at the time of closest approach.

Contents

1 Introduction

1.1 Comets

Comets are often referred to as "icy-conglomerates" (Festou et al., 2004). They are irregularly-shaped bodies made up of ice and rock. This is as opposed to asteroids, which are mostly made up of rock and metals and are found much closer to the Sun. When a comet get to within 5 AU its ice begins to sublimate (or "outgas") due to its interaction with to solar radiation. When it approaches to within 3 AU, the rate of outgassing becomes sufficiently large such that it can be seen as the comet's tail (Dones et al., 2004).

The icy-rock that undergoes this outgassing is known as the cometary nucleus which is surrounded by a thin atmosphere called the coma. Comets also have two so-called cometary tails (see Figure 1). One tail is made of gas and the other of which is made of dust. The gas is more easily accelerated by solar wind than the dust which is what cause the spitting of the two tails. More is known about the chemical composition of the coma and tail than the nucleus. Measurements of the coma have shown near-solar abundances for all but the lightest elements and most volatile compounds, such as N_2 (A'Hearn, 2004). The most abundant compound ejected from the comet is H_2O, which dissociates (either through photo or electron impact dissociation) into H, O, and OH which make up most of the comet's tail (Festou et al., 2004; Feldman et al., 2015).

The most recent major cometary observations were performed by the Rosetta mission in which the Rosetta space probe manoeuvred into an orbit around comet 67P, remaining in orbit for 17 months. A notable finding from this mission was the discovery of a three times higher deuterium to hydrogen ratio in the comet's coma than the one found on earth. This is evidence against the idea that earth got its water from comets (Altwegg et al., 2015). Another notable finding was that the observed HI, OI, and CI emission lines are produced by electron impact disassociation of H_2O and CO_2 (Feldman et al., 2015). These electrons are produced by the photodissociation of H_2O. The emission lines were previously thought only to be produced through photodissociation. This revealed the dominant mechanism through which the H, O, OH, and C ions are produced in the coma.

A comet's orbit can be defined with six "keplerian" orbital elements: the semi-major axis (a) and the eccentricity (e) together define the shape of the orbit; the inclination (i), the longitude of the ascending node (Ω), and the argument of periapsis (ω) define the orientation of the orbit in space; and the true anomaly (f) defines the position of the comet along its orbit. All these orbital elements can be seen in Figure 2.

The semi-major axis is defined as one of the two continuous lines which runs from the centre of the ellipse, over one of the foci, and terminates at one of the two points on the edge of the ellipse furthest from the centre. The eccentricity is a measure of how elongated the ellipse is. It is defined as the ratio between the length of the line from the centre of the ellipse to the foci to the length of the semi-major axis. The inclination is the angle at which the orbit is tilted away from a reference plane, in the case of the solar system this is the ecliptic plane: the plane at which the earth orbits the Sun. The longitude of the

Figure 1: Comet Hale-Bopp with a gas tail on the left and a dust tail on the right, taken on the 4^{th} of April, 1997 at the Johannes-Kepler-Observatory, Austria. Image credit: E. Kolmhofer and H. Raab.

ascending node defines the second possible tilt of the orbit in space. There are two nodes in the body's orbit, defined as the points where the orbit crosses the reference plane. The ascending node is the node through which the body travels "upwards" through the reference plane. Which direction is upwards is convention. The longitude of the ascending node is then the angle between a reference direction and the ascending node. For heliocentric orbits, this reference direction is usually the vernal equinox. The argument of periapsis defines the last possible tilt of the orbit in space. It is defined as the angle between the ascending node and the perihelion (see following paragraph). Finally the true anomaly is defined as the

angle between the perihelion and the position of the orbiting body.

Two other relevant parts of the orbit are known as the perihelion and aphelion. The perihelion is the point of the orbit at which the comet is closest to the centre of mass of the system. The aphelion is the point of the orbit at which it is furthest. Both points can be seen in Figure 2.

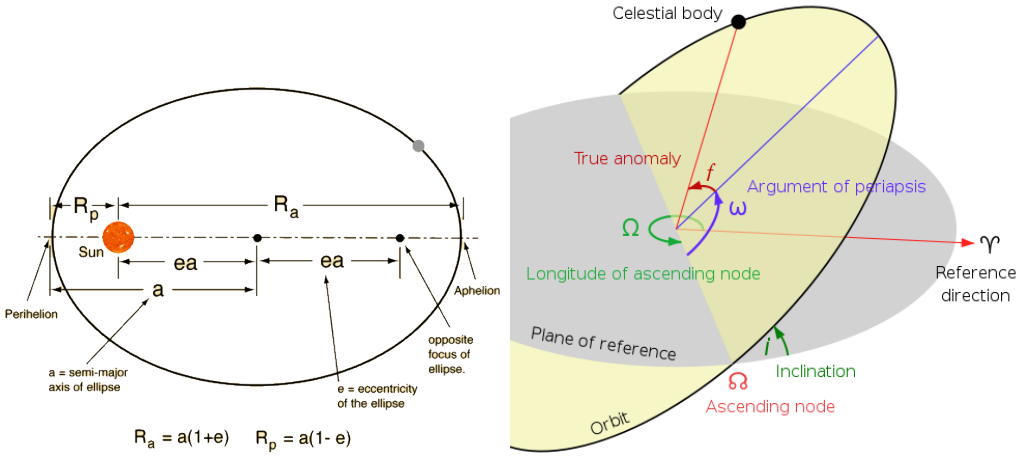

Figure 2: These two sketches together show all of the keplerian orbital elements. The semi-major axis and eccentricity can be seen in the image on the left (as well as the perihelion and aphelion) and the true anomaly, inclination, argument of periapsis, and longitude of the ascending node can be seen in the image on the right. Image credits: *Left:* By Emily Lakdawalla, the planetary society. *Right:* By Wikipedia user "Lasunncty". Creative commons licence: CC BY-SA 3.0. Note: The symbol for true anomaly was altered in this image from ν to f.

Comets are classified into different"families" based on observed differences in their orbits. They are divided into Jupiter-family comets (JFCs) and Nearly Isotropic Comets (NICs). The dividing line between the two is at a semi-major axis of $a = 7.4$ AU, with JFCs falling below that line and NICs falling above it. The basis for this dividing line is that JFCs' orbits are heavily influenced by Jupiter's gravity (Dones et al., 2004).

NICs are further divided into Halley-Type Comets (HTCs) and Long Period Comets (LPCs) with the dividing line between the two of these being at $a = 40$ AU, with HTCs falling below that line and LPCs falling above it (Dones et al., 2004). The dynamical basis for this dividing line is that HTCs will enter mean-motion resonance with Jupiter at some point while LPCs will not, as demonstrated by Chambers (1997).

1.2 New comets and the Oort cloud

Before 1950, there was a paradox caused by the existence of "new" comets. "New" comets are comets with a semi-major axis, $a > 10^4$ AU. They are called "new" because any comets

with such a large semi-major axis are very weakly bound so that their gravitational interaction with the planets will either take away an average energy of ΔE, making it bound to a much smaller orbit, or give it the energy ΔE, turning its orbit unbound so that it will never return to the inner solar system. This means that an observation of such a comet would likely be first time it has observed, hence the term "new" comet. This meant that such comets shouldn't exist. Despite this, they were still observed.

As a solution to this paradox, the Oort cloud was theorised by Oort (1950). The Oort cloud provided an explanation of the appearance of "new" comets: it was a reservoir of icy-conglomerates that orbit the Sun at very large distances: 50,000 to 150,000 AU was Oort's estimate. These extreme distances, coupled with how frequently we observe comets, imply that the population of this reservoir must be enormous: Oort's estimate was 10^{11} comets, which is still in line with modern estimates placing it between $10^{10} - 10^{12}$.

Upon a gravitation perturbation which maybe be due to a passing star, a molecular cloud, or the galactic tidal force (Festou et al., 2004), some of the icy-conglomerates may be perturbed such that their perihelion (q) is reduced to below 3 AU at which distance the tail can be seen (Dones et al., 2004).

1.3 Structure of the Oort cloud

Estimates of the number of comets in the Oort cloud vary around $10^{10} - 10^{12}$. Estimates of the inner edge go as low as $a = 2,000$ AU and of the outer edge go as high as $a = 200,000$ AU. The Oort cloud's comets are not directly observable at such distances due to their small size and low brightness. We must thus instead make inferences about the Oort cloud's structure from evolutionary models, simulations, and from observations of comets that enter the inner solar system.

Using only the latter of those would not be enough because there is a bias to which comets enter the inner solar system such as the so-called "Jupiter barrier" which prevents most comets in the Oort cloud with a semi-major axis of $a < 2-3\times10^4$ AU reaching the inner solar system. The Jupiter barrier having this effect is due to (1) Jupiter's strong gravity which can either take enough energy to shift a comets orbit to a much lower orbit or supply enough energy to make a comet unbound, in combination with (2) a strong dependency of the change in perihelion (experienced due to the galactic tide or stellar perturbation) of $\Delta q \propto a^{7/2}$. Because of Jupiter's strong influence on its orbit, a comet is much more likely to be observed if the Δq it experiences places the comet past the reach of Jupiter's gravity. And because of the strong dependency of Δq on a, comets with lower semi-major axes are harder to shift down to lower perihelia and are thus less likely to experience a Δq high enough to place it past Jupiter's influence. Levison et al. (2001) found $a \gtrapprox 28,000$ AU to be the condition for a comet to be able to experience a jump from $q = 10$ AU to $q = 3$ AU, a jump which would by-pass the orbits of Jupiter and Saturn as well as make the observable.

The structure of the Oort cloud can be described by the distribution of the keplerian

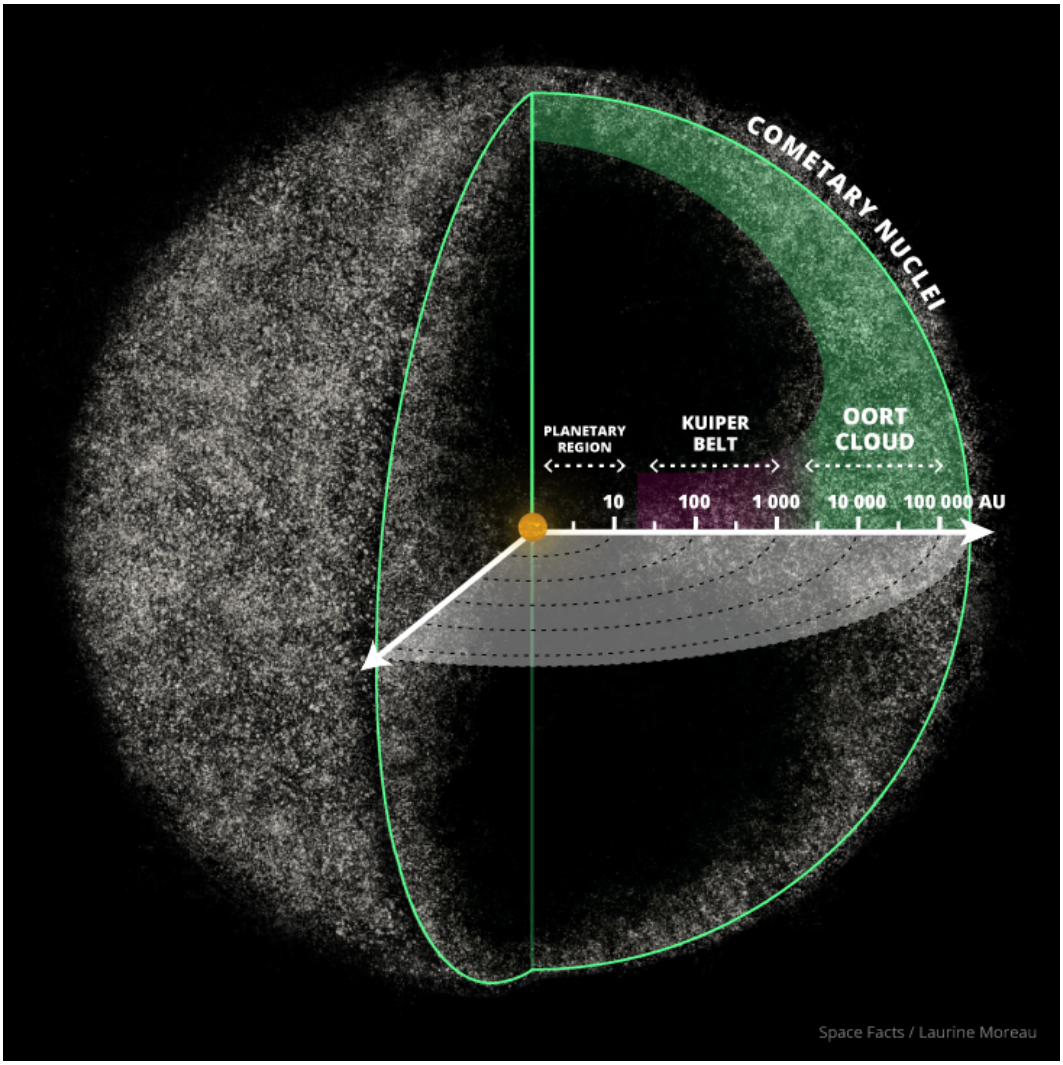

Figure 3: Sketch of the solar system with the radial component in log scale. Image credits: laurinemoreau.com via Space Facts.

orbital elements.[1] The argument of periapsis, longitude of the ascending node, and inclination can all be selected such that there is a spherically symmetric distribution of comets. This would be expected since the cometary orbits were randomised by stellar encounters (Dones et al., 2004). Since the true anomaly describes the comet's position along its orbit, it will be distributed uniformly in time-spent at different parts of the orbit. This means that regions of the orbit through which comets travel faster, such as regions close to the perihelion with $f \approx 0$, will have fewer comets at a particular point in time than a region through which comets travel slower, such as regions close to the aphelion with $f \approx \pi$.

[1] See §1.1 for a description of the keplerian orbital elements.

Because the Oort cloud has never been directly observed, we have to rely on theory and simulations to infer the distribution of the semi-major axis and eccentricity.

Rickman et al. (2008) ran a Monte Carlo simulation of the Oort cloud over the lifetime of the solar system (4.5 Gyr) and included the galactic tide and stellar encounters. They used an a distribution found by Duncan et al. (1987) who used another Monte Carlo simulation: 3×10^3 AU $< a < 1 \times 10^5$ AU with number density $n(a) \propto a^{-1.5}$. However, Rickman et al. find that this distribution is not stable: the outer comets are lost at a faster rate than they can be replaced by the inner Oort cloud and the distribution's number density dependency changes to $n(a) \propto a^{-2}$.

Higuchi and Kokubo (2015) used the classical impulse approximation[2] to see how the spherical Oort cloud evolved from a planetesimal disk due to stellar encounters. They ran the simulation for 10 Gyr: more than twice the age of the solar system. They found that, within at least 5 Gyr, the resulting structure of the Oort cloud had a semimajor axis distribution which climbed to a peak at $a = 3 \times 10^4$ AU and then dropped off outwards as $n(a) \propto a^{-2}$, petering out at $\sim a = 1 \times 10^5$ AU. This distribution was independent of the initial distribution of the planetesimal disk, meaning that this is likely to be the current a distribution of the Oort cloud. They don't explicitly define an inner edge to the Oort cloud: their distribution peaks at $a = 3 \times 10^4$ AU and then drops to 0 at $a = 0$.

Higuchi and Kokubo (2015) found the eccentricity distribution to be $n(e) \propto e$. Dones et al. (2004) stated that the eccentricity has a median value of 0.7, which is also the median value of a $n(e) \propto e$ distribution between 0 and 1.

1.4 *Gaia* DR2

Gaia is a satellite that was launched in 2013. It aims to map the position and velocity of over 1 billion (or 1%) of the Milky Way's stars. Data Release 2 (DR2) was released in 2018. The DR2 data contained 7.2 million sources with a known radial velocity, making those stars fully defined in 6 dimensional position-velocity space (Gaia Collaboration et al., 2016, 2018).

1.5 Stellar encounters and interstellar comets

Stellar encounters happen when two stars interact gravitationally and change each other's velocity vectors. There are two types of encounters: strong encounters and weak encounters. A strong encounter is defined as an encounter for which the change of the potential energy at closest approach is equal to or greater than the stars' initial kinetic energy. This implies

[2]The classical impulse approximation is when a comet considered to be fixed relative to the Sun and the change in velocity it experiences due to a passing star is given by: $\boldsymbol{\Delta v} = \frac{2GM_*}{\boldsymbol{V}_*}\left(\frac{\hat{\boldsymbol{b}}_c}{b_c} - \frac{\hat{\boldsymbol{b}}_*}{b_*}\right)$ where M_* is the mass of the star, $\boldsymbol{V}_*$ is the velocity vector of the star relative to the Sun, $\boldsymbol{b}_c$ is the vector pointing from the comet to the star's closest approach to it, and $\boldsymbol{b}_*$ is the vector pointing from the Sun to the star's closest approach to it (Rickman et al., 2005).

that the change in velocity experienced by the star will be of the order of the initial velocity. A weak encounter is one in which the initial path of the stars are barely affected.

Stellar encounters can be very important in the randomisation of motion (or "relaxation") of stars in a galaxy and can have a significant impact on an individual star's trajectory.

Stellar encounters also have a significant impact on the evolution of the Oort cloud or presumably any other star's potential comet cloud too. Comet clouds have not been observed around other stars but they may exist since individual comets and cold debris belts have been observed around other stars. Beust et al. (1990) has also shown that that variation in the metallic absorption lines in the spectrum of the debris disk of the star Beta Pictoris is commensurate of models of evaporating star-grazing comets with high eccentricities. This has been observed in the debris disks of other stars and is considered by some to be indirect evidence of the existence exocomet clouds (Hanse et al., 2018).

Note that in this paper, "comet cloud" will refer to shell of comets around any star whereas "the Oort cloud" will only be used to refer to the Sun's comet cloud.

Hanse et al. (2018) ran a simulation over the lifetime of the Sun, including the galactic tide and stellar encounters, and found that between 25 and 65%[3] of the Oort cloud's mass had been lost over its life time due mainly to stellar encounters. $\gtrapprox 80\%$ of the mass loss was due to encounters with a minimum encounter distance of ~ 200 AU.

This mass is lost from the Oort cloud either by comets getting ejected directly into interstellar space or being injected into the planetary region. Only 5% of "new" comets which enter the planetary region will make it back to the Oort cloud. Of those that don't make it back to the Oort cloud, half become bound to a tighter orbit by perturbations from Jupiter and the other gas giants and the other half become unbound and are also ejected into interstellar space (Dones et al., 2004). This presumably happens to the comet clouds of other stars too, potentially being a mechanism which populates interstellar space.

1.6 Gliese 710

Gliese 710 is a star with a stellar classification of K7V (Gray et al., 2006). V means that it is a main sequence star − it is still in the initial phase of its lifetime where its core is fusing hydrogen into helium. K is the spectral type below the Sun's spectral type of G meaning that Gliese 710 is cooler than the Sun. It has a mass of 0.6 times the mass of the Sun (García-Sánchez et al., 1999).

De la Fuente Marcos and De la Fuente Marcos (2018) found, using Gaia DR2 data, that an encounter between the Sun and Gliese 710 is expected to take place in 1.35 Myr with a closest approach of $\sim$ 13,400 AU. It is the closest future stellar encounter that we know of. And it is a very close encounter: by comparison, the closest know past encounter ("Scholz's

[3]The high uncertainty in this number is due to the high uncertainty in the Sun's past galactic path. There is a much higher mass-percentage loss if the Sun migrated outwards from its birth cluster to its current orbit than if it migrated inwards

Star") was found to have a closest approach of 52,000 AU (Mamajek et al., 2015). Of future encounters, Bailer-Jones et al. (2018) found 694 stars among 7.2 million in the Gaia DR2 data that had at least a 50% chance of coming within 10^6 AU of the Sun and only 7 coming within 10^5 AU in the next 15 Myr.

It is not known whether Gliese 710 has a comet cloud or not. But it is known that minor bodies like comets form in protoplanetary disks, which can then potentially be launched into a comet cloud by the star's planets. There is no reason to believe this would not have happened to Gliese 710 too.

1.7 The galactic tide

The galactic tide is a force experienced in the solar system due to the gradient of the Milky Way's gravity across the length of the solar system. This is much the same as lunar and solar tide experienced by the Earth.

The galactic tide is able to increase the semi-major axes of comets once a comet's orbit has been cast out of the planetary zone by one of the planets and is thought to be the mechanism through which comets get out to Oort cloud distances (Dones et al., 2004). It is not, however, able to randomise the distribution of stars into the spherically symmetric distribution which the Oort cloud is thought to have. This is instead done by stellar perturbations (Higuchi and Kokubo, 2015).

Rickman et al. (2008) ran three simulations of the Oort cloud over 5 Gyr: one that only included the galactic tide, a second that only included stellar perturbations, and a third that included both of them. They found that 132% more comets' perihelia were perturbed to within 5 AU of the Sun over the 5 Gyr in the simulation that only included stellar perturbations than for the simulation that only included the galactic tide. They also found a synergy between the galactic tide and stellar perturbations: there were 70% more comets whose perihelia were perturbed to within 5 AU in the simulation that simulated both effects than there were in the sum of the two simulations that simulated the effects by themselves.

1.8 This study

It is of interest how the Sun's future encounter with Gliese 710 will affect the Oort cloud: how many comets are transferred to the inner solar system, how many are ejected into interstellar space, and how the structure of the Oort cloud is affected by the encounter. Comparing the percentage of comets transferred to the inner solar system in projects like this one and coupling this with the number of comets observed, for instance, could inform estimates of the population of the Oort cloud.

It is possible that Gliese 710 also has a comet cloud, the effect on which may also be interesting. Thus we simulated the Oort cloud of our Sun and of a hypothetical comet cloud around Gliese 710 with the aim of investigating how the comet clouds' structures are affected by the stellar encounter.

2 Method

2.1 The N-body simulator

To study the close encounter, we used an N-body simulator. N-body simulations are often used to study dynamical systems of particles under the effects of forces like magnetism or gravity. This makes it appropriate for simulating comet clouds: an arbitrary number of test particles can be initialised and integrated through time. A disadvantage of the use of an N-body simulator is that non-gravitational forces cannot be taken into account. Non-gravitational forces are relevant to the orbits of comets: outgassing applies a non-gravitational force to the comet which affects its orbit. We will, however, be predominantly dealing with comets at distances further than $r = 5$ AU where outgassing does not occur so this is not a significant issue.

The N-body simulator we chose to use for this project is called `REBOUND`. It was written in `C` but has a `Python` module which was the version we used (Rein and Liu, 2012). We chose to use it because it was open source and had the versatility to run the simulations needed in this project. The `REBOUND` package also has several integrators, we chose to use the `MERCURIUS` variable time-step integrator which increases the time-step of the simulation when possible to save on computing time.

2.2 Initial conditions: comet clouds

We initialised the orbits of the comets by randomly selecting the six keplerian orbital elements[4] from appropriate distributions.

We selected the argument of periapsis (ω), longitude of the ascending node (Ω), and inclination (i) in such a way as to create a spherically symmetric comet cloud. To do this, i needs to be selected uniformly in $cos(i)$. Simply selecting uniformly in i would result in a crowding of points at the poles because i is a latitudinal angle. Since ω and Ω are longitudinal angles, they are selected uniformly in the range $[0, 2\pi]$.

The true anomaly (f) defines the comet's position along its orbit. It must thus be selected uniformly in how long it spends at any point of its orbit. This is to ensure that there is not, for example, an initial clustering of comets in the centre of the Oort cloud because true anomalies close to the Sun were over represented in sampling.

To do this we derived a relationship between f and v. We know that $v = \sqrt{GM\left(\frac{2}{r} - \frac{1}{a}\right)}$. This is the vis-viva equation where G is the gravitational constant, M is the mass of the body being orbited, and r is the radial distance of the orbiting body from the parent body. We also know that $r = \frac{a(1-e^2)}{1+e\cos(f)}$. Therefore:

$$v = \sqrt{GM\left(\frac{2 + 2e\cos(f)}{a(1-e^2)} - \frac{1}{a}\right)} \tag{1}$$

[4] See §1.1

Having that, we assigned $1/v(f)$ as a proxy for time spent in the region of the orbit corresponding to the true anomaly value f. This is valid because the faster a particular part of the orbit is travelled through, the less time is spent there (this can be shown through Kepler's second law). Selecting uniformly in $1/v$ thus yields an f-distribution that is stable through time. We did this with a numerical inverse transform.

We calculated 10^5 v-values between 0 and 2π. We then inverted all the v-values to $1/v$, summed them cumulatively, and then normalised the resulting cumulative distribution by dividing everything by the maximum of the distribution. Then we selected a random number between 0 and 1 in the normalised cumulatively summed $1/v$ distribution and then found the equivalent f-value using Equation 1. We also subtracted the minimum $1/v$ value from the rest of the $1/v$ distribution. It was necessary to do this because the comet would otherwise over-sample f in the region closer to the perihelion; this would make the distribution unstable as when integrating there would be an initial net outwards movement of the comets.

The resulting distribution can be seen in Figure 4. In the figure we can see the evolution of the Sun's comets' true anomaly over time. As can be seen in Figure 4, the initial distribution evolves over time, but the peaks both remain at $f = \pi$ and $f = -\pi$. The initial minimum of 0 comets at $f = 0$ rises to ~ 100 comets in a bin of size ~ 0.25, or $\sim 10\%$ the height of the peaks by 2×10^5 yr. This remains stable through to 8×10^5 yr. Gliese 710's hypothetical comets showed this same trend when simulated.

In selecting the parameters of the semi-major axis (a) distribution, we referred to Higuchi and Kokubo (2015)'s and Rickman et al. (2008)'s studies mentioned in the introduction. Both found a distribution of $n(a) \propto a^{-2}$ with independent methods.[5] They also agree on the outer boundary of the Oort cloud being at $a = 1 \times 10^5$ AU. We chose to use these two parameters. The point at which we should start the $n(a) \propto a^{-2}$ distribution is less constrained, with Higuchi and Kokubo (2015)'s distribution peaking at $a = 3 \times 10^4$ AU and then dropping to 0 at $a = 0$ and Rickman et al. (2008)'s starting at 3×10^3 AU. We chose $a = 5 \times 10^3$ AU because it lies between these two values.

We used inverse transform sampling to generate the initial distribution of the comets' semi-major axes. We used $n(a) \propto a^\gamma$ as a proxy for the cumulative distribution function.

This yields a (normalised) cumulative distribution function of:

$$F(a) = \frac{\int_{a_{inner}}^{a} n(a')da'}{\int_{a_{inner}}^{a_{outer}} n(a')da'} = \frac{\int_{a_{inner}}^{a} a'^{\gamma} da'}{\int_{a_{inner}}^{a_{outer}} a^{\gamma} da'} = \frac{\left[\frac{1}{\gamma} a'^{\gamma+1}\right]_{a_{inner}}^{a}}{\left[\frac{1}{\gamma} a'^{\gamma+1}\right]_{a_{inner}}^{a_{outer}}} = \frac{a^{\gamma+1} - a_{inner}^{\gamma+1}}{a_{outer}^{\gamma+1} - a_{inner}^{\gamma+1}}$$

Where $F(a)$ is the cumulative distribution function of the number of comets as a function of the semi-major axis, a; a_{inner} is the inner semi-major axis limit of the comet cloud; a_{outer} is the outer limit; and γ is power of the number distribution, $n(a)$.

[5] Higuchi and Kokubo (2015) simulated the evolution of the Oort cloud using classical impulse approximation and found that independent of the initial a-distribution, it always evolved into a distribution with a dependency $n(a) \propto a^2$ within 5 Gyr. Rickman et al. (2008) ran a Monte Carlo simulation of the Oort cloud over the age of the solar system (4.5 Gyr) with a semi-major axis distribution of $n(a) \propto a^{-1.5}$. This distribution evolved to $n(a) \propto a^2$ by the end of the simulation. See §1.3, page 8 for more details.

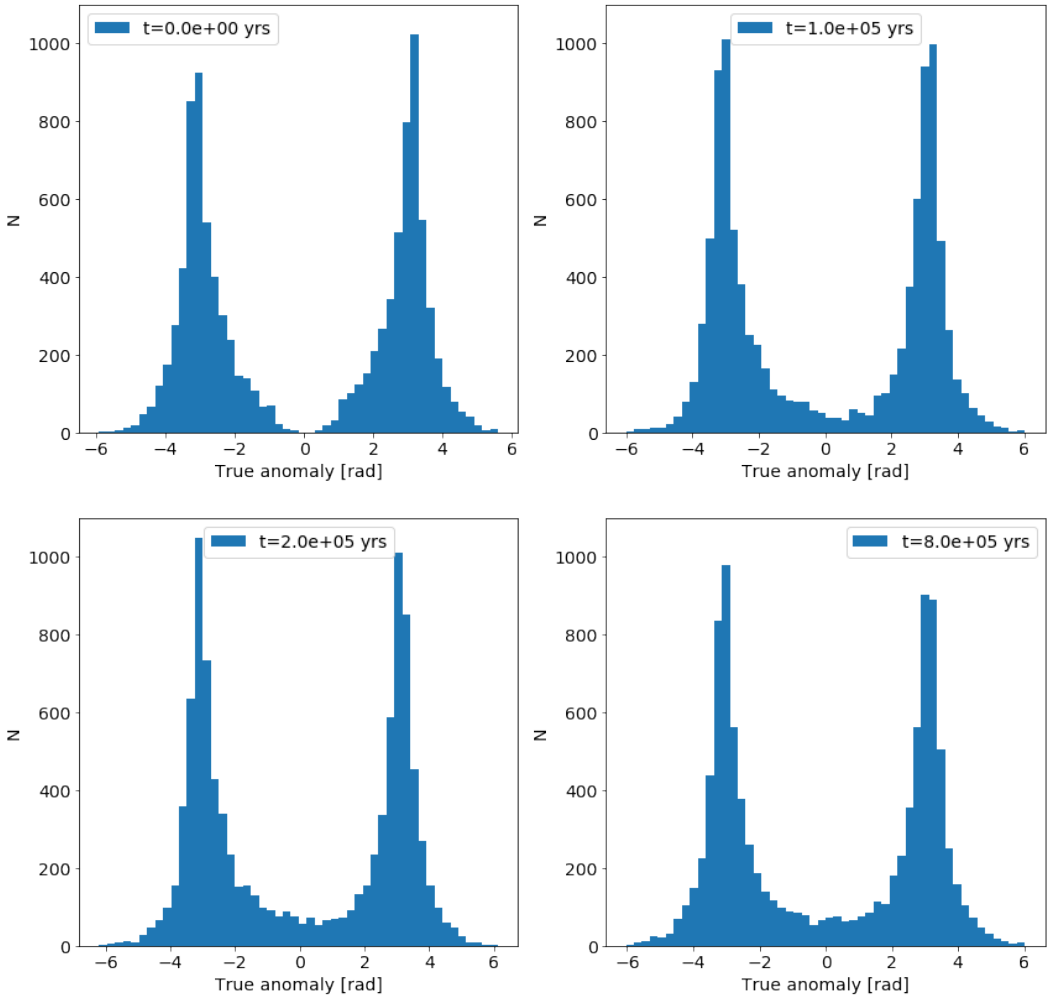

Figure 4: The true anomaly distribution of the Sun's comets at t=0 yr, 100,000 yr, 200,000 yr, and 800,000 yr.

The inverse cumulative distribution function of this is (if $F(a) \equiv x$, $a \equiv F^{-1}(x)$):

$$F^{-1}(x) = \left(x(a_{outer}^{\gamma+1} - a_{inner}^{\gamma+1}) + a_{inner}^{\gamma+1}\right)^{\frac{1}{\gamma+1}} \tag{2}$$

Since $F(a)$ is normalised, sampling uniformly in x in the range $[0, 1]$ for $F^{-1}(x)$ leads to the desired distribution.

We set $\gamma = -2$ because of the agreement in this value between Higuchi and Kokubo (2015) and Rickman et al. (2008).

For the distribution of eccentricities we used the distribution described in Higuchi and Kokubo (2015). The results of their 10 Gyr simulation showed a $n(e) \propto e$ distribution, the

median of which agreed with the median cited by Dones et al. (2004). We thus chose to use this as the distribution of eccentricities.

Another relevant parameter to choose for the simulation is a cut-off point for the perihelion of the comets in the Oort cloud. This is because once a comet is in a planet-orbit-crossing path, interactions dramatically changing the orbit of the comet can take place: it could, for example be ejected from the solar system or be moved to an orbit fully in the planetary region. Since we are not including the planets in the simulation, we should make sure that none of the comets are initially in that region. Rickman et al. (2008) make a similar choice in their project and set the cut off point to be $q > 32$ AU. This is a reasonable distance to define it at with Neptune's aphelion being 30.3 AU. Thus, a and e are selected such that comets with a $q < 32$ AU are discarded.

We also realised we had to scale down Gliese 710's comet cloud by some factor. A body of a lower masses will not be able to keep an object gravitationally bound to it at distances as far out as bodies of a higher mass will be able to. The Hill sphere is a useful concept here. The Hill sphere is a region around an astronomical body within with an object of a certain mass, eccentricity, and semi-major axis can be bound. The radius of the Hill sphere of a lower-mass body relative to a higher-mass body (r_H) has a dependency on the lower mass (m) and the higher mass (M) as approximately $r_H \propto \left(\frac{m}{M}\right)^{1/3}$. This means that the Hill sphere's radius of the lower-mass body will be smaller the smaller m/M is. This motivates scaling down Gliese 710's comet cloud.

The way we decided to scale down Gliese 710's comet cloud was by making the assumption that the Sun's Oort cloud's comets and Gliese 710's comet cloud's comets would have roughly the same binding energy to their stars. This is a reasonable assumption to make, as the Sun and Gliese 710 will have undergone similar stellar encounters in their life time, meaning that their comets will be bound with roughly equal binding energy, U. We can then find a relationship between the inner and outer radii of the two comet clouds using the standard gravitational potential energy equation:

$$U = -\frac{GMm_c}{R}, \tag{3}$$

$$U_{Sun} = U_{Gliese}, \tag{4}$$

$$\Rightarrow \frac{GM_{Sun}m_c}{R_{Sun}} = \frac{GM_{Gliese}m_c}{R_{Gliese}}, \tag{5}$$

$$\Rightarrow R_{Gliese} = \frac{M_{Gliese}}{M_{Sun}} R_{Sun} = 0.6R_{Sun}, \tag{6}$$

Where G is the gravitational constant, m_c is the mass of the comet, M_x is the mass of star x, and R_x is the distance between the comet and the star for star x.

Thus, we scaled down the inner and outer edges of Gliese 710's comet cloud's semi-major axis distribution by a factor 0.6, as well as the minimum allowed perihelion.

2.3 Initial conditions: the Sun and Gliese 710

We utilized *Gaia* DR2 to determine the position and velocity of Gliese 710 (Gaia DR2 4270814637616488064) prior to its close encounter with the Sun. The integration was performed with the `Python` package `Galpy` (Bovy, 2015). The adopted galactic potential is the `galpy` three-component axisymmetric smooth `MWPotential2014` described in Bovy (2015). We took the position of the Sun in the galactic Cartesian frame to be (X, Y, Z) $= (-8.13, 0, 0.02)$ kpc (Gravity Collaboration et al., 2018; Bennett and Bovy, 2019). We adopted the value of the local standard of rest $(U, V, W) = (11.1^{+0.69}_{-0.75}, 12.24^{+0.47}_{-0.47}, 7.25^{+0.37}_{-0.36})$ km s^{-1} (Schönrich et al., 2010a). The heliocentric distance of Gliese 710 was determined by the inverse parallax method. To calibrate the parallaxes we applied a systematic offset of 0.029 mas (Lindegren et al., 2018).

The initial coordinate and velocity values we got from this can be seen in Table 1. These values are listed in the equatorial frame as they would be on January 1st 2000 (J2000).

Parameter	Sun	Gliese 710
x [AU]	0.157829	-12144.5
y [AU]	-2.53622	255023
z [AU]	-0.0981803	11013.4
v_x [AU/yr]	0.00196010	1.29330
v_y [AU/yr]	-0.00242372	-14.4543
v_z [AU/yr]	-0.00110646	-0.477820

Table 1: x, y, z coordinates and v_x, v_y, v_z velocity components of the Sun and Gliese 710 derived with the method outlined in this section.

2.4 The integration

We ran two integrations which we will refer to as Simulation 1 and Simulation 2. The parameters of these simulations can be seen in Table 2. Simulation 1 ran for 4 Myr with 10,000 comets in each comet cloud and a time-step of 1 yr in order to investigate changes to the large scale structure of the comet clouds. We run Simulation 2 for 80,000 yr with 100,000 comets and a time-step of 0.01 yr to be able to more accurately simulate the effect on individual comets which come too close to the perturbing star to accurately simulate with an integration time-step of only 1 yr.

The time at which we determined the position and velocity of Gliese 710, as described in the previous subsection, was 100,000 yr before the minimum distance of the encounter. We then integrated the Sun and Gliese 710 backwards 1.5 Myr to get the coordinates for Simulation 1. This was done to ensure the comet clouds had "settled" from any imperfectly sampled initial orbital parameters, such as true anomaly which takes $\sim 2 \times 10^5$ yr to settle, as seen in Figure 4. We also integrated the Sun and Gliese 710 forwards $\sim$ 63,000 yr for Simulation 2. We selected the exact time to start Simulation 2 by plotting the orbital

Name	Total integration time (T)	Number of comets (per comet cloud)	Time-step	Time of minimum distance (relative to beginning of simulation)
Simulation 1	4 Myr	10,000	1 yr	1.6 Myr
Simulation 2	80,000 yr	100,000	0.01 yr	37,000 yr

Table 2: Parameters of the two simulations. Both integrated with the `MERCURIUS` integrator.

elements, perihelia, and aphelia of individual comets from Simulation 1 over time.[6] These orbital parameters were constant for nearly the entire 4 Myr except for a short time of $\sim 20,000$ yr to either side of the time of the minimum distance of the encounter. We chose the times of the Simulation 2 such that all the activity seen in the Simulation 1 was fully enclosed in the Simulation 2. There is no need extend the integration far into the future: there is no external force on the comets in this simulation besides that of the penetrating star's gravity. This means that when the comets' orbits have stopped being affected by the penetrating star's gravity (as judged by the change in orbital parameters in the aforementioned plots of Simulation 1's orbital parameters over time), their orbits do not change and the orbital parameters remain constant (except, of course, true anomaly). After running Simulation 2, we verified that the orbital parameters are at a constant value by the time the simulation ends. This is evidenced in Figure 12. The paths of these two simulations can be seen in Figure 5. Table 2 shows the integration parameters for both simulations.

[6]The equivalent graphs for Simulation 2 can be seen in Figure 8.

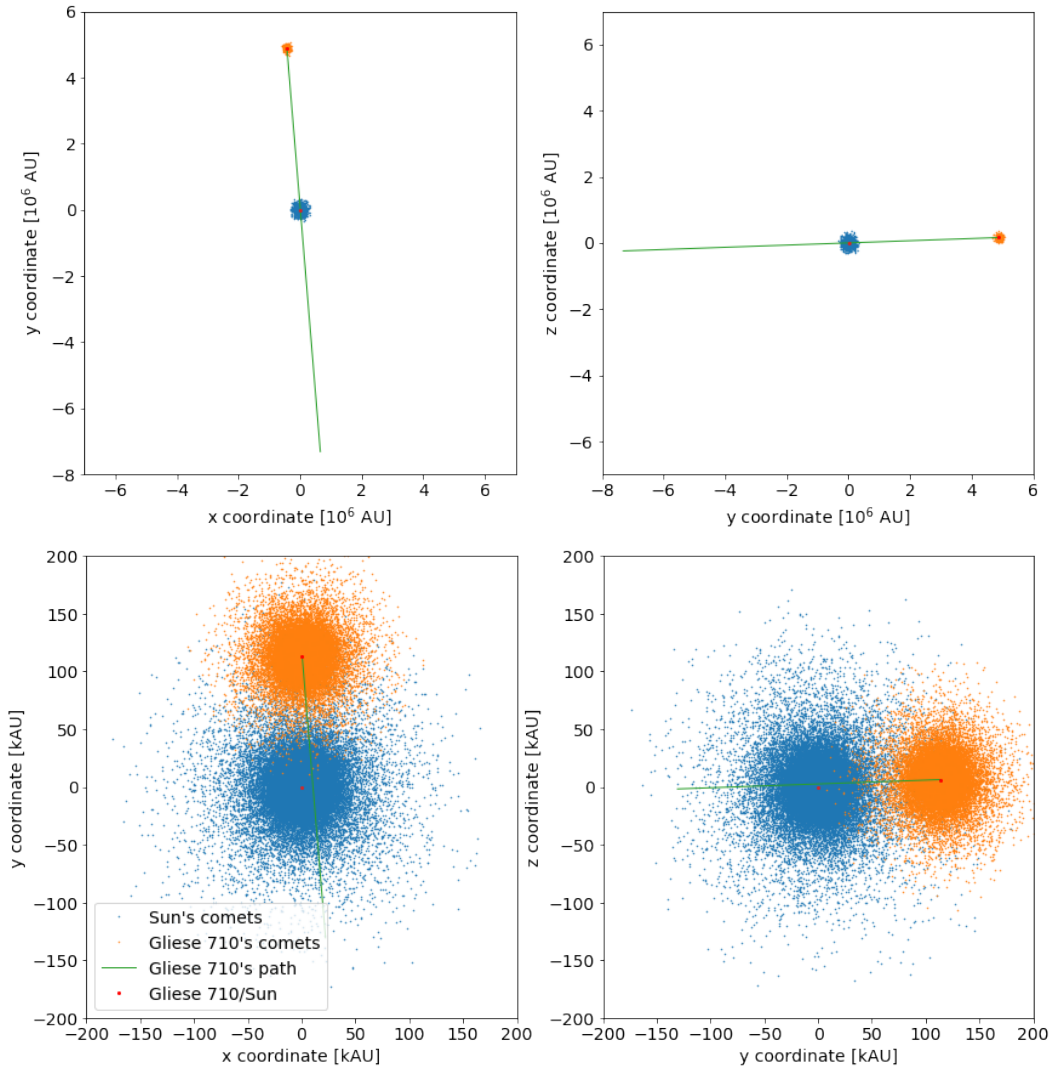

Figure 5: *Top right and left:* The position of the two comet clouds at the beginning of Simulation 1. *Bottom left and right:* The position of the two comet clouds at the beginning of the Simulation 2. The line in green shows Gliese 710's path in every plot.

3 Results

We have defined $-1/a$ as a proxy for energy: $E \equiv -1/a$, as done by Dones et al. (2004) – though they used $E = 1/a$, reversing the conventional sign of energy. $-1/a$ can be validly used as a proxy for the energy because as the semi-major axis increases, the comet is less gravitationally bound to its star and thus its energy has decreased (as has $-1/a$). When the semi-major axis is negative, the comet is unbound, and the energy is positive. This will

be used to identify comets which have become gravitationally unbound. Thus, for the rest of this paper "energy proxy" refers to $-1/a$.

The minimum encounter distance was 12,312 AU for Simulation 1 and 10,828 AU for Simulation 2. These are off by 8.12% and 19.2% respectively from the distance found by De la Fuente Marcos and De la Fuente Marcos (2018). This offset is more reasonable when converted to angular offset in trajectory from Gliese 710's current position. The angular offset is 2.80×10^{-4} rad for Simulation 1 and 6.62×10^{-4} rad for Simulation 2. The resulting ratio of difference in gravitational force between the two objects is given by $F_1/F_2 = R_2^2/R_1^2$. Thus, the error in Simulation 1 produces a gravitational force 1.18 times too high and the error in Simulation 2 produces a gravitational force 1.53 times too high.

Figure 6 shows the mean and median r-values of both the Sun's and Gliese 710's comets for Simulation 1. This was plotted to show the change the large scale structure of the Oort cloud; the average and median r-values for Simulation 2 showed changes that were small and probably due to noise and stabilisation which is why Simulation 1 was used instead for this figure.

The full r-distributions for both stars in Simulations 1 and 2 can be seen in Figure 7.

Figure 8 shows the change in perihelion and aphelion of 10 comets from each star of the 200,000 simulated in Simulation 2. This was plotted to show the varying changes experienced by individual comets and how that change relates to the time of the minimum distance. And indeed, a variety of patterns of change can be seen in these plots. Some of the changes are centred after the time of minimum distance such as the aphelion of the Sun's comet number 30000 (seen in red) which is centred at $t \sim 40,000$ yr. Others, however, such as the perihelion of Gliese 710's comet number 70000 (grey) is centred around the minimum distance ($t \sim 37,000$ yr). Some comets such as Gliese 710's comet number 70000 (grey)'s aphelion change is unidirectional while other comets' changes are bidirectional such as the Sun's comet number 40000 (purple) perihelion change.

The plots of the semi-major axis, the eccentricity, and the inclination over time all share similar characteristics to the plots of the perihelion and aphelion: the individual comets have constant a, e, and i values for most of the plot with the same variety of changes to those values described in the paragraph above. More illuminating are the the histograms in Figure 9.

The histograms show the differences in perihelion, aphelion, semi-major axis, eccentricity, inclination, and the energy proxy of all the comets from Simulation 2. These differences are calculated by subtracting the initial values from the final values for each parameter for each comet. The resulting numbers were then binned into 400 different bins and plotted in Figure 9. The range of the histograms has also been adjusted to a range that cuts off some far-flung comets for clarity.

All of the histograms in Figure 9 have a mode of 0, showing that the most common "change" experience by a comet was no change. The Sun's distributions are more peaked for the difference in perihelion, aphelion, and semi-major axis, where as the Gliese 710's distributions are more spread out for the eccentricity, inclination and energy proxy. The

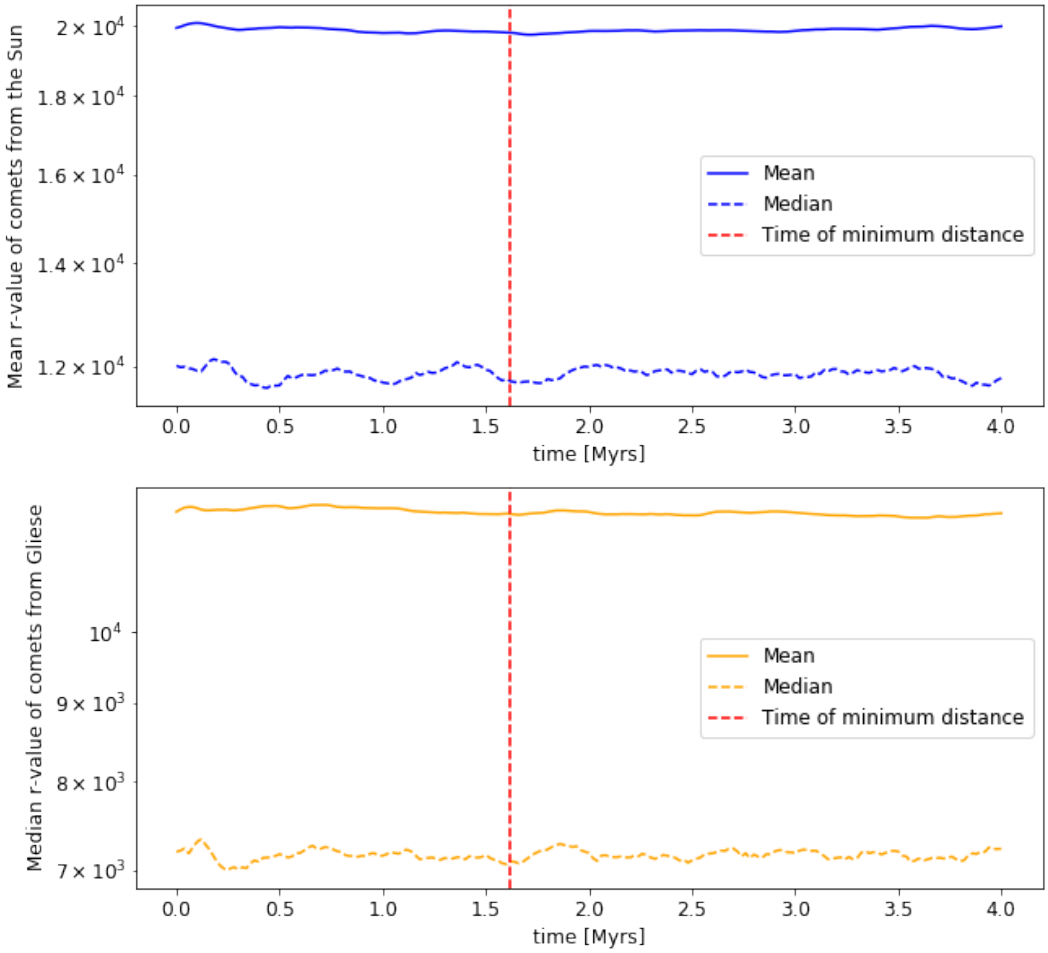

Figure 6: The mean and median r-values of the 10,000 Sun's comets in Simulation 1.

full width half-maximum (FWHM) of all these graphs can be seen in Table 3. The greater the FWHM, the more those parameters were changed by the encounter. The most dramatic difference between Gliese 710 and the Sun can be seen in the bottom right histogram in Figure 9 of the energy proxy change, followed by the middle left histogram of the semi-major axis change. A difference in FWHM between the eccentricity and inclination cannot be seen in Table 3 despite one existing as seen by the difference in spread in Figure 9. This is because the bin-size limits the resolution of the distribution. Increasing number of bins beyond 400 increased the noise and gave the distribution a false maximum.

Note also the incredibly small change in inclination. The most extreme comets experience a change $\Delta i = 0.1$ which is only $\sim 3\%$ of their theoretically possible change of $\Delta i = \pi$. This tells us the the inclination is a hard parameter to change.

The change in the semi-major axis can also be seen in Figure 10. The distribution of

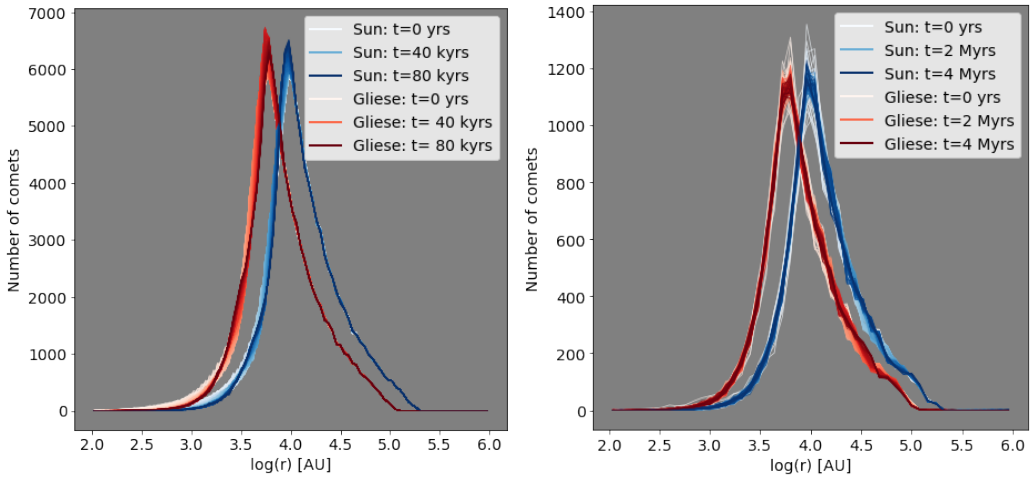

Figure 7: The r number distribution in log space for Simulations 1 and 2

Parameter	FWHM, Sun	FWHM, Gliese 710
Perihelion [AU]	10	7.5
Aphelion [AU]	22.5	20
Semi-major axis [AU]	107.5	72.5
Eccentricity	0.007	0.007
Inclination [rad]	0.003	0.003
Energy proxy [AU^{-1}]	0.0023	0.0052

Table 3: The FWHM of the distributions seen in Figure 9.

the Oort cloud remains the same for semi-major axes of $\sim a < 5 \times 10^4$ AU for the Sun and $\sim a < 3 \times 10^4$ AU for Gliese 710. Beyond that there's a spreading of a to higher values, up to $\sim 1.025 \times 10^5$ AU for the Sun and $\sim 6.15 \times 10^4$ AU for Gliese 710. These are both a 2.5% increase in the maximum semi-major axis values seen in the graph of the comet clouds respectively. Note also that, for clarity, the range of these plots have been limited to not show unbound comets or the rare comets that get large semi-major axes: 146 (0.15%) of the Sun's comets and 591 (0.59%) comets reached semi-major axes beyond positive range of the plot.

Also of interest are the $E = -1/a$ distributions seen in Figure 11 because of how easily unbound comets can be seen in this figure. The figure shows the distributions in $-1/a$ for the Sun's and Gliese 710's comets for Simulation 2 at the beginning and end of the simulation. Both plots in Figure 11 have a uniform distribution of energy at $t = 0$. After the encounter, a few comets can be seen to have become unbound, with less of the Sun's comets becoming unbound than of Gliese 710's. Some spreading to lower energies can also be seen in the Sun's distribution.

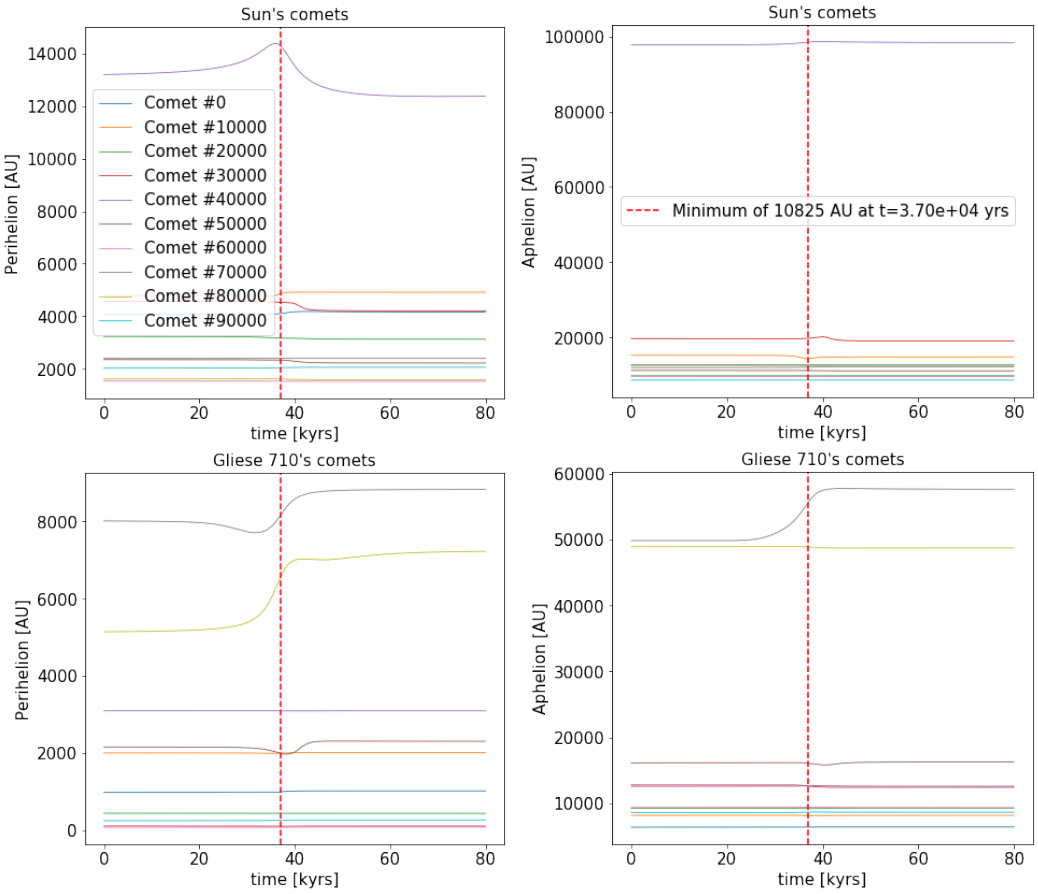

Figure 8: A sample of the Sun's and Gliese 710's comets' perihelion and aphelion plotted over time.

A total of 70 of the 200,000 comets became unbound in this simulation: 0.035%. Of the 70 comets, 50 of them (71%) had initial energies in the upper half of the initial energy distribution. Of the 70 ejected comets, 19 (0.019% of Sun's total comets) were the Sun's and 51 (0.051% of Gliese 710's total comets) were Gliese 710's.

The comets whose perihelia were shifted to within planetary range are of interest. Of the 100,000 comets around each star, 98 (0.098%) of the Sun's and 121 (0.12%) of Gliese 710's comets' perihelia entered the planetary region of $r < 32AU$: a total of 219 comets. Of the Sun's 98 comets entering the planetary region, 5 (0.005%) of the comet's perihelia come within 3 AU of the Sun, where a cometary tail becomes visible. Of the 98 of the Sun's comets that entered the planetary region, 50 of them (51%) were initially in the lower half of the energy distribution. Of Gliese 710's 121 comets, 97 (80%) were initially in the lower half of the energy distribution.

Adding up the numbers of comets that are ejected into interstellar space and the number

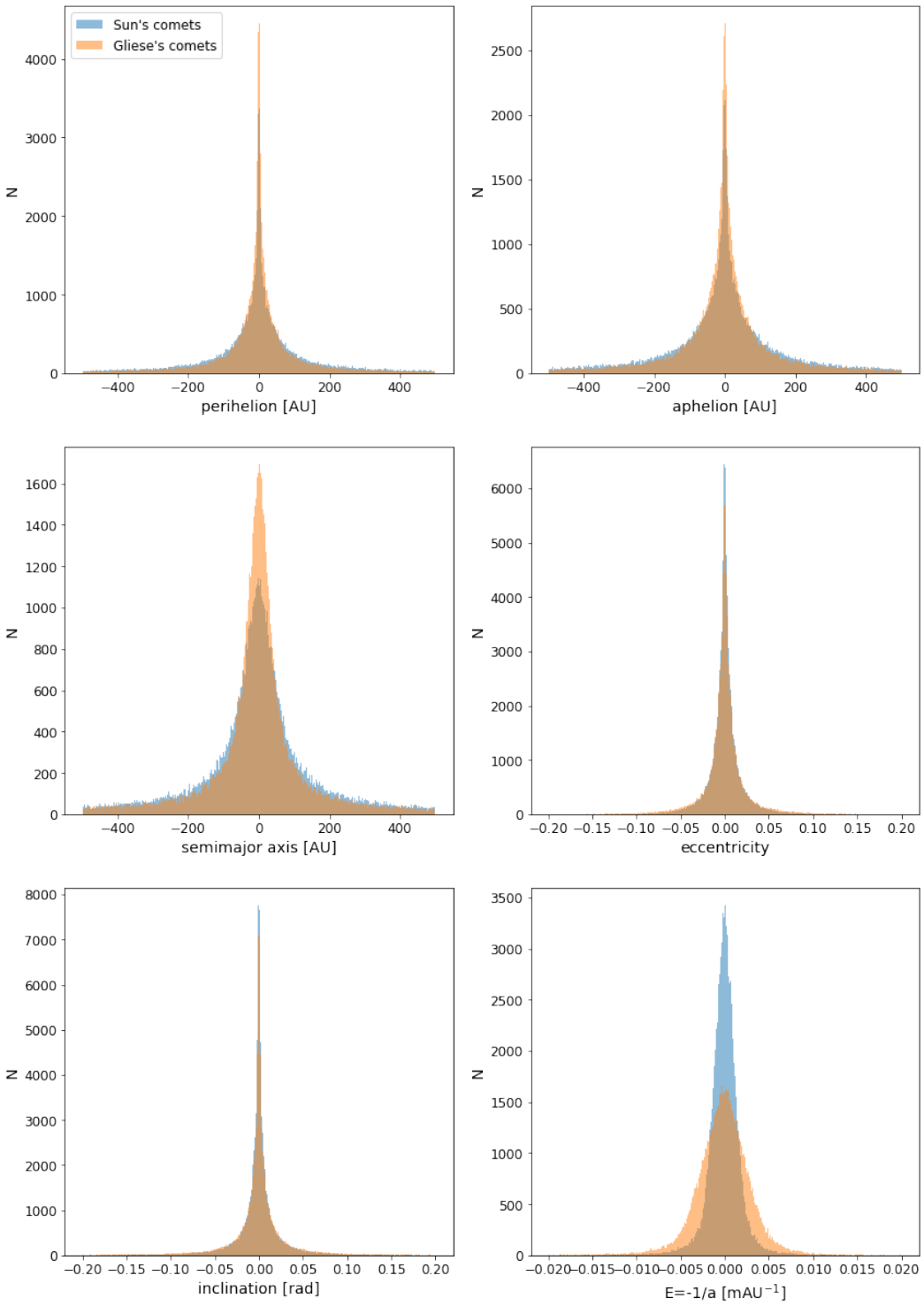

Figure 9: The differences in perihelion, aphelion, semi-major axis, eccentricity, inclination, and the energy proxy, $-1/a$. The differences shown are the difference in value from the beginning to the end of the simulation.

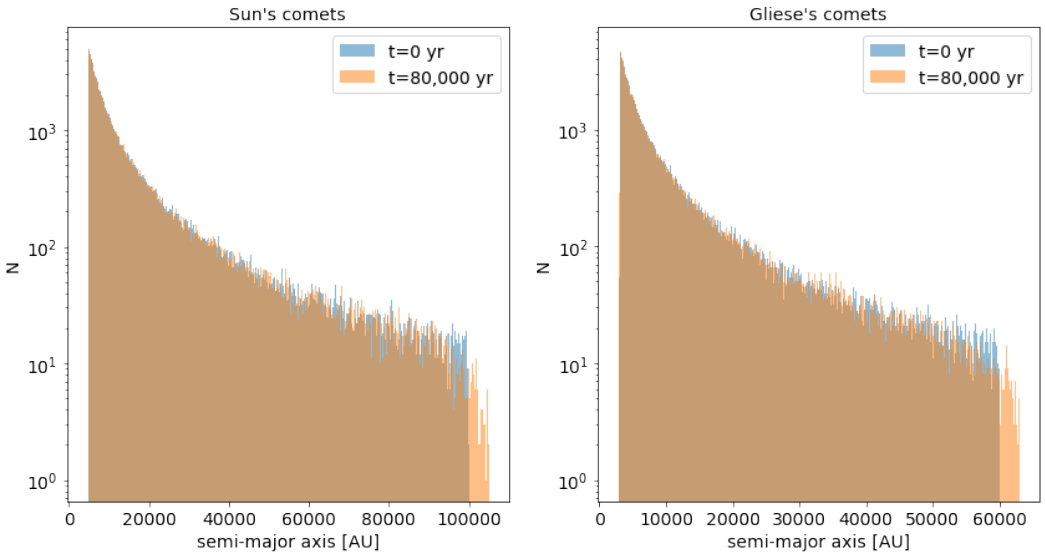

Figure 10: The distribution of the semi-major axes of the Sun's comets (left) and Gliese 710's comets (right) plotted at both the beginning and end of Simulation 2.

of comets which enter the planetary zone gives 117 (0.117%) of the Sun's comets which are no longer part of the Oort cloud and 172 (0.172%) of Gliese 710's comets. This assumes that all comets entering the planetary zone are no longer part of the Oort cloud. A similar assumption was made by Rickman et al. (2008). Of course, this will not truly be the case so any results derived from this will be an upper limit.

This gives a percentage number loss of 0.117% for the Oort cloud and 0.172% for Gliese 710's comet cloud. Let us take this encounter with Gliese 710 to be an order of magnitude approximation to the effect of the standard encounter with a loss of 0.1% of the Oort cloud's population. This seems reasonable as an order of magnitude approximation as, although the encounter with Gliese 710 is very close, it is also very fast and Gliese 710 is only a fraction of the Sun's mass which diminishes its effect on the Oort cloud (Feng and Bailer-Jones, 2015). Bailer-Jones et al. (2018) found, using Gaia DR2 data, 7 stars with a 50% probability of coming within 0.5 pc of the Sun ($\sim 10^5$ AU) in the next 15 Myr.[7] We can thus take the encounter rate to be 3.5 per 15 Myr, or ~ 0.23 per 1 Myr. This translates to an approximately 20% oort cloud population loss over the next Gyr. This is our upper bound. Repeating this calculation assuming that only comets which were directly ejected into space are lost from the Oort cloud, we get a 4.3% population loss over the next Gyr. This is our lower bound.

The median changes in a, e, i, and $E = -1/a$ over time can be seen in Figure 12. The median was used instead of the mean because the mean was affected by outlying comets

[7]They estimated the encounter rate to be ~ 20 per Myr for a distance of 1 pc, but those stars do not penetrate the Oort cloud and so this simulation cannot be considered representative of them.

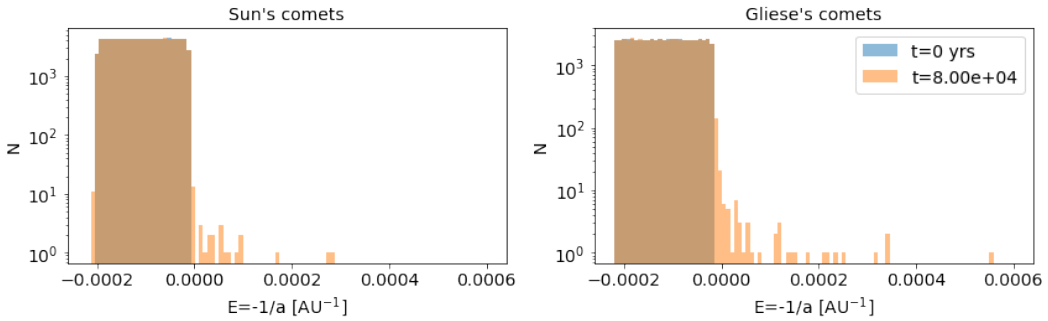

Figure 11: Histogram of the energy proxy showing the distribution in -1/a for the Sun on the left and Gliese 710 on the right. Both graphs show the distribution at $t = 0$ and $t = T = 80,000$ yr.

that become unbound and dominated the shapes of the lines. The median doesn't have this problem. The change was calculated by summing all the differences in the relevant parameter between one output of the simulation and the next. The solid lines show the median change of the relevant parameter and the dotted lines the absolute median change of the relevant parameters. As you can see, the change in time peaks around the time of minimum distance for all plots. There is a slight preference for a positive change for the semi-major axis and the aphelion at the peak, with $\sim 51.7\%$ (a positive bias of 1.7%) of the median change in semi-major axis being positive for the Sun's comets and ~ 52.4 % (a positive bias of 2.4%) being positive for Gliese 710's comets at the time of minimum distance. We will from now on refer to the bracketed positive bias numbers as Positive Bias at Peak of the encounter (PBP) for clarity and brevity. The aphelia of the Sun's comets have a PBP of 0.75% and Gliese 710's a PBP of 1.2%. The PBP of all the other orbital parameters (including ones not shown in Figure 12) can be seen in Table 4.

Parameter	Positive Bias at Peak of encounter (PBP), Sun	Positive Bias at Peak of encounter (PBP), Gliese 710
Semi-major axis	1.7%	2.4%
Aphelion	0.75%	1.2%
Perihelion	0.075%	-0.0013%
Eccentricity	0.14%	0.81%
Inclination	-0.0096%	0.023%
Energy proxy $(-1/a)$	2.2%	3.0%

Table 4: The percentages of comets whose change of orbital parameters was positive at the time of closest approach subtracted by 50%: we have called this the Positive Bias at Peak of the encounter (PBP), "Peak" referring to the peaks seen in Figure 12 that occur approximately at the time of minimum distance of the encounter.

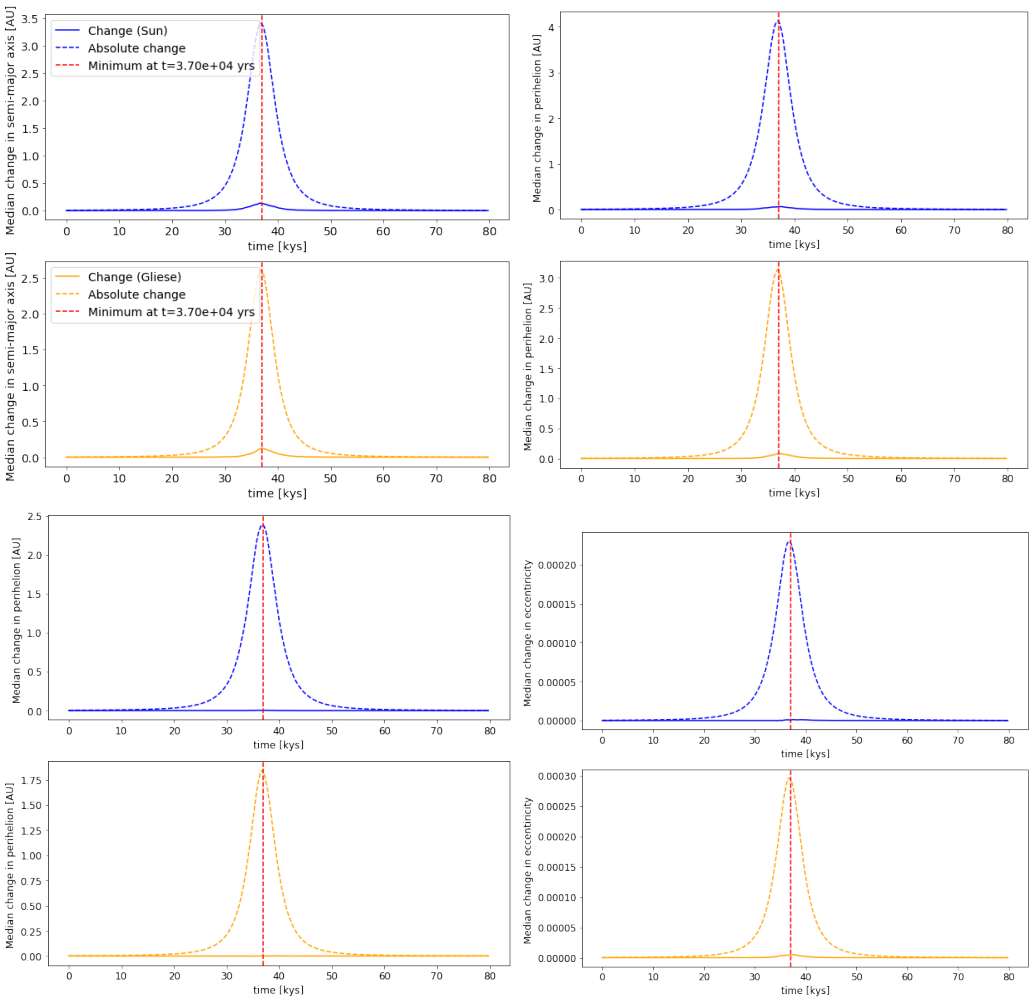

Figure 12: Median changes in semi-major axis, aphelion, perihelion, and eccentricity over time.

To illustrate the change in the comets' orbits, we plot the semi-major axis against the eccentricity. These plots can be seen in Figure 13. It is clear that the initial hard boundary of the semi-major axis at 10^5 AU does not remain hard: 209 (0.21%) of the Sun's comets and 591 (0.59%) of Gliese 710's comets' semi-major axes go above their respective initial hard boarders. Comets at higher semi-major axes also have higher eccentricities: comets at semi-major axes of 2×10^5 AU or more are found mostly at eccentricities between 0.9 and 1 (the y-axis has been limited in Figure 13 for clarity). 12 (0.012%) of the Sun's comets went above 1.5×10^5 AU, 11 (92%) of which had an eccentricity greater than 0.9. 31 (0.031%) of Gliese 710's comets reached higher than 1.5×10^5 AU, 17 (55%) of which had an eccentricity greater than 0.9.

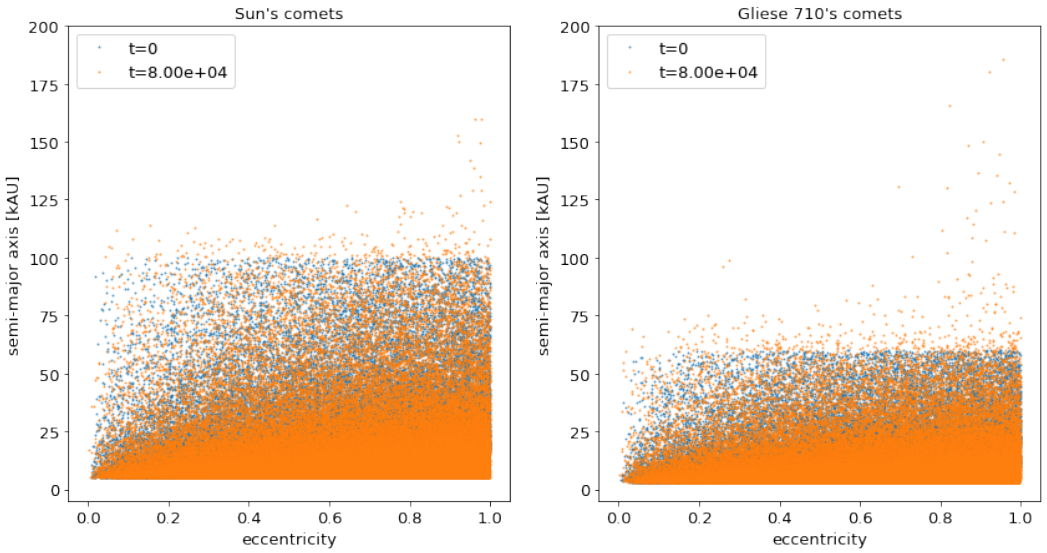

Figure 13: The eccentricity plotted against the semi-major axis of the Sun's (left) and Gliese 710's (right) comets for Simulation 2. Values at plotted at the beginning and end of the simulation.

The eccentricities pre- versus post-encounter were also plotted as a further illustration of the change in eccentricities experience by the comets. This can be seen in Figure 14. The spread of eccentricities is greater for Gliese 710's comets as seen by the increased deviation from the $e_{before} = e_{after}$ line. More of Gliese 710's comets also reach eccentricities > 1 (became unbound) after the encounter and more of its comets are perturbed to higher eccentricities too. There is also no visible correlation between how eccentric these unbound comets become and the initial eccentricity. Eccentricities between $\sim$ [0.2,0.8] are roughly equally as deviated from the $e_{before} = e_{after}$ line, but more extreme eccentricities close to $e = 0$ and $e = 1$ experience less change, as seen by the narrowing of the spread near these extremes.

The semi-major axes pre- versus post-encounter were also plotted and can be seen in Figure 15. There seems to be no correlation we can draw from these plots between a_{before} and a_{after} for the comets whose semi-major axis reaches $a > 10^5$ AU after the encounter. We can, however, see an increase in deviation from the $a_{before} = a_{after}$ line with an increase in a, with a barely visible spread for the lowest a-values.

The energy proxies ($E = -1/a$) pre- versus post encounter were plotted and can be seen in Figure 16. An increased deviation from the $E_{after} = E_{before}$ line as E increases can again be seen. There is also an increase in the number of comets which become unbound as the initial energy increases; there are no comets which become unbound which had energies lower than $\sim -1.7 \times 10^{-4}$ AU^{-1} in either plot.

The distribution of the velocities of the unbound comets relative to their host-star at

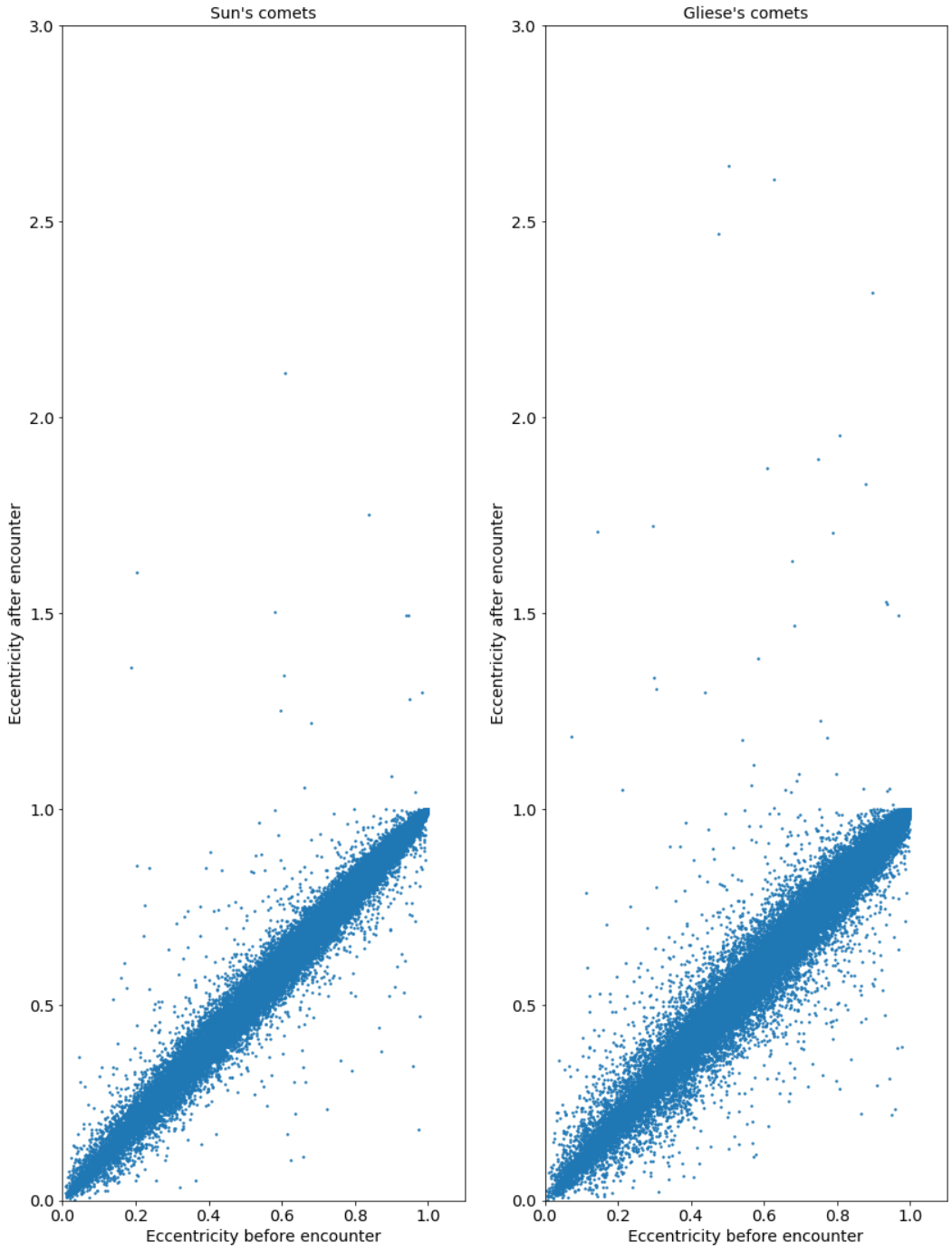

Figure 14: The eccentricity pre- versus post-encounter for all of the Sun's and Gliese 710's comets. Seen on the left and right respectively.

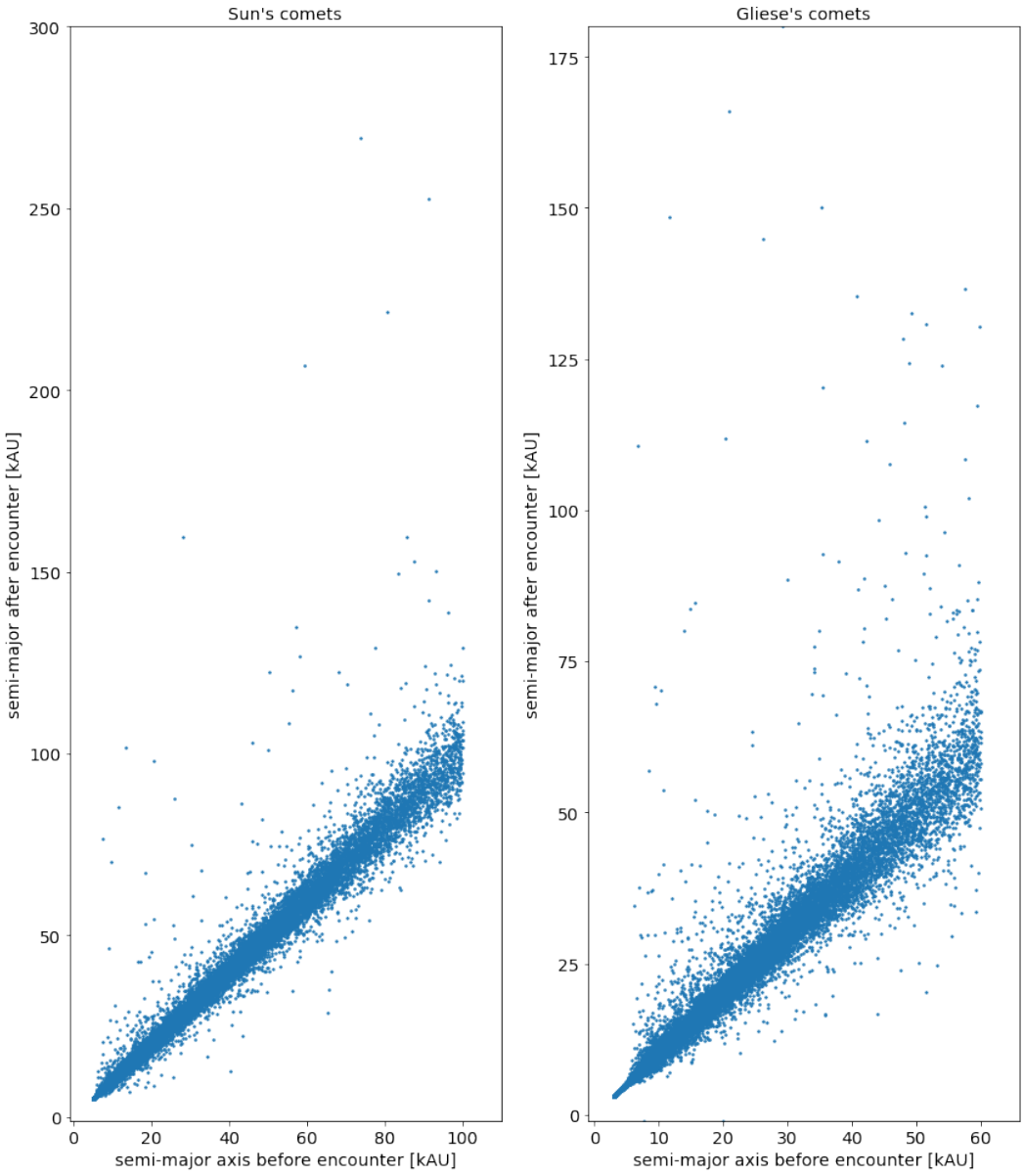

Figure 15: The semi-major axis pre- versus post-encounter for all of the Sun's and Gliese 710's comets. Seen on the left and right respectively. Note the different scales of the x- and y- axes of the two plots.

the end of Simulation 2 was binned with 35 bins and plotted in a histogram, seen in Figure 17. The Sun's comets have a higher velocity distribution with a peak at ~ 0.09 AU/yr, with Gliese 710's comets having a peak at ~ 0.075 AU/yr.

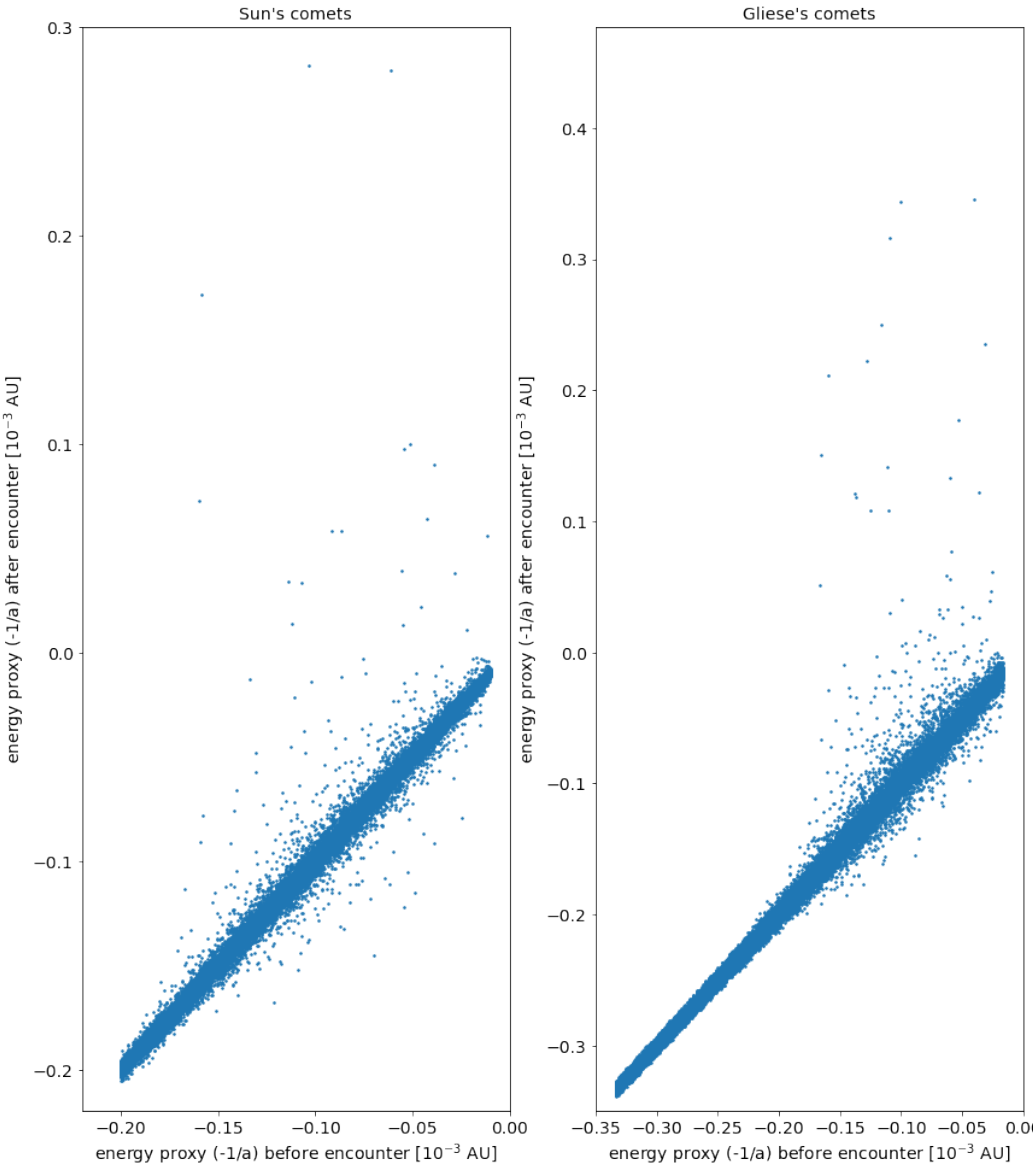

Figure 16: The energy proxy $(-1/a)$ pre- versus post-encounter for all of the Sun's and Gliese 710's comets. Seen on the left and right respectively. Note the different scales of the x- and y- axes of the two plots.

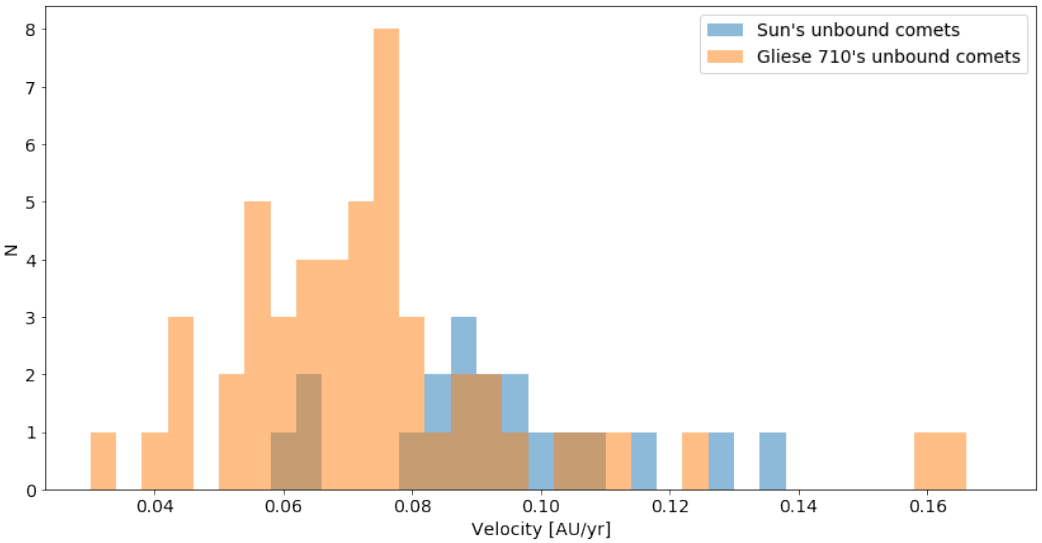

Figure 17: The velocity distribution of the unbound comets.

4 Discussion

4.1 Deviation of minimum encounter distance from literature value

There was a deviation in the minimum encounter distance of 8.12% for Simulation 1 and 19.2% for Simulation 2 from the distance found by De la Fuente Marcos and De la Fuente Marcos (2018). This is an error likely due to a mistake in an insufficient time-step or in inaccurate or improperly initialised coordinates of the Sun and Gliese 710: the coordinates of the Sun and Gliese 710, derived as described in §2.3 and seen in Table 1, were derived by integrating the current-day position and velocities of the Sun and Gliese 710 in only the galactic potential and not the gravitational interaction of the two stars with any other stars or each other.

This deviation may not have a significant affect on the effects of this encounter. When converted to log space, Festou et al. (2004)'s minimum distance value is 4.12 AU, Simulation 1's value is 4.09 AU, and Simulation 2's value is 4.03 AU. These values deviate from each other by 0.09 AU at most in log space. Looking at these values on the x-axes of the plots in Figure 7 shows that this is not a significant deviation in terms of number density. All of these $\log(r)$ values correspond to $\sim$ 6000 comets in a bins of size 0.04 AU in log space. Gliese 710 will thus travel through areas of roughly equal number density, meaning the deviation of the minimum encounter distance from the literature value should not affect the number of the Sun's comets interacts strongly with. This is one way that a deviation from the true minimum encounter distance may influence our results that has here been shown to be negated.

4.2 Change in large scale structure

Figures 6 and 7 illustrate that there is no large scale change in either of the comet cloud's structures or populations because of this encounter. This is to be expected when Hanse et al. (2018) found that 80% of the mass that was lost in the Oort cloud's life time was by encounters with a minimum encounter distance of $\sim$ 200 AU while Gliese 710's minimum encounter distances in these simulations were $\sim$ 10,800AU and 12,300 AU.

4.3 Comets ejected from the comet clouds

We found a 0.117% population loss of the Oort cloud in Simulation 2. Results from Bailer-Jones et al. (2018) implied a loss per Gyr of 4.3% to 20%. Hanse et al. (2018) found that if the Sun hadn't migrated radially through the galactic disk over its 4.5 Gyr lifetime (meaning roughly the same stellar density as the present), it would have lost 46% of its mass, giving an average loss of $\sim$ 12% per Gyr. However, Hanse et al. (2018) also found that 80% of that mass that was lost was due to encounters with a minimum encounter distance of $\sim$ 200 AU. This leaves only a potential 2.4% loss per Gyr for all other encounters greater than this minimum encounter distance, only some of which will have been due to encounters like Gliese 710's. This calls into question the assumptions made when calculating the 4.3% to 20% mass loss per Gyr. Perhaps the other 2.5 encounters with a minimum distance of less than $\sim 10^5$ AU in the next 15 Myr (see §3, page 23) are not accurately represented by this simulation. Or perhaps the Sun's current local stellar density is higher than the average past stellar density of the Sun's path in Hanse et al. (2018)'s paper. The percentage of comets lost from the Oort cloud has also been inflated by the assumption that all comets whose perihelia falls into the planetary range are lost. The decreased minimum encounter distance is also likely relevant in the inflation of this number. And of course, this project simulated only a single encounter and thus generalising the results of this is a little dangerous. The upper bound of 20% was calculated with the assumption that all comets which become unbound from the solar system and all comets whose perihelion enters the planetary region are lost from the Oort cloud. The lower bound of 4.3% was calculated assuming that only comets which become directly unbound from the solar system are lost from the Oort cloud. The lower bound being much closer to the 2.4% value inferred from Hanse et al. (2018) implies that the assumption made for the calculation of the lower bound is more accurate. Thus we can infer that most comets whose perihelia enter the planetary region will return to the Oort cloud.

Gliese 710's higher percentage of comet loss − particularly by comet ejection, having $\sim$ 2.68 times more comets ejected than the Sun − may be due to the fact that in this simulation there was an equal number or comets in each cloud, but Gliese 710's comet cloud was 0.6 times the radial size, increasing the number density of comets by $\sim 1/(0.6^3) \approx 4.63$, approximating the comet cloud as a full sphere. Where as the distance traversed though the cloud by the penetrating star only decreases by a factor of $\sim$ 0.6, meaning an increase of encounters by a factor $1/(0.6^3) \times 0.6 \approx 2.78$. The discrepancy between this factor and the factor of 2.68 found in this simulation is may be due to noise from a too small sample size of

ejected comets: we only have 70 comets that were ejected so the percentage of comets that would be ejected from each comet cloud if they had the full $\sim 10^{11}$ population of the Oort cloud might be different. It may also be in inaccuracies in the approximations used, such as that the number density scales as the volume of a sphere despite it being a thick shell. may also be the source of error. Running more simulations, or running another simulation with more comets would reduce the noise in the percentage of comets ejected in an encounter like this one.

The discrepancy between the factors of 2.68 and 2.78 may be further explained by the fact that the scaling of the comet clouds means that Gliese 710's comets experience a lesser gravitational pull from the Sun relative to their pull from Gliese 710 and vice-versa. This is because $g \propto M/R^2$ and both M and R scaled with the same factor of 0.6 in this simulation. This makes Gliese 710's gravitational pull on its comets a factor of $1/0.6$ stronger. At closest approach, the ratio of the Gliese 710's gravity to the Sun's gravity is 4.06 for a comet at the inner edge of Gliese 710's comet cloud at the point were the line between the Sun and Gliese 710 intersects with inner edge of Gliese 710's comet cloud. An equivalent comet in the Sun's comet cloud has a ratio of the Sun's gravity to Gliese 710's of 2.24.

4.4 Perturbations of the cometary orbital parameters (over time)

Figures 8 and 12 show that most of the change occurs around the time of the encounter. The relatively flat solid lines in Figure 12 which show the median change experience by a comet in the comet clouds through time show is; as does the symmetry around 0 in Figure 9 which shows the distribution of difference in initial and final values of various orbital parameters. From these two figures, it is apparent that the vast majority of the changes cancel each other out. This further confirms that (and explains why) there is no significant large scale change to the Oort cloud's structure.

However, there is still a net increase in the comets' semi-major axes, as seen by the feature in the solid line at the time of the minimum distance in the two top left subfigures in Figure 12. The solid line is the median change of the semi-major axis of the comets. The peak of this bump corresponds to a PBP of the semi-major axis of $\sim 1.7\%$ for the Oort cloud. The Sun's comets aphelia have a PBP of 0.75%. The reason for this is likely due to the fact that, for a given impulse, the semi-major axis and aphelion will undergo a larger increase than decrease. This can be shown using the following equations:

$$r_p = a(1 - e) \tag{7}$$

$$v = GM\left(\frac{2}{r} - \frac{1}{a}\right) \tag{8}$$

Where r_p is the perihelion, v is the velocity of the comet relative to its star, and all the other variables are as previously defined.

Setting $r = r_p$ in Equation 9 and thus $v = v_p$ (the velocity at perihelion) then replacing r_p in this equation for the expression for r_p in equation 7 gives the proportionality: $v_p^2 \propto 1/a$.

From Equation 7 we have $a \propto r_p$, thus:

$$v_p^2 \propto \frac{1}{a} \propto \frac{1}{r_p} \tag{9}$$

We can now say, for a ratio between an increase and decrease in the velocity at perihelion squared, $(\Delta v_p^2)_{+/-}$, for a change in velocity at perihelion Δv_p due to the effect of a stellar passage:

$$\frac{|(\Delta v_p^2)_+|}{|(\Delta v_p^2)_-|} = \frac{v_p^2 - (v_p + \Delta v_p)^2}{v_p^2 - (v_p - \Delta v_p)^2} < 1, \text{ for } \Delta v_p > 0 \tag{10}$$

Equation 10 shows that a positive change in velocity at the perihelion will increase v_p^2 less than a negative change in velocity at the perihelion will decrease it. Since $v_p^2 \propto \frac{1}{a} \propto \frac{1}{r_p}$, a decrease in v_p^2 increases a and r_p and vice-versa. This means that a and r_p will increase more for a decrease in v_p than they will decrease for an increase in v_p – or, a and r_p are more easily perturbed to higher values than lower values. The degree to which the aphelion and semi-major axis increase is dependant on the true anomaly of comet. These will most easily increase most relative to an increase in v at the perihelion and lease at the aphelion.

The aphelia of the comets in the Oort cloud have a PBP of 0.75% whereas their perihelia only have 0.075% and their eccentricity has a change of 0.14%. We can infer from this that the comets that were drawn outward by Gliese 710's passage, increasing their aphelion and eccentricity with a practically fixed perihelion. This means that the semi-major axis, eccentricity, and aphelion are relatively easier to increase from a stellar encounter.

Figure 9 and Table 3 show that there is a consistently wider spread of changes in the perihelion, aphelion, and semi-major axis for the Sun's comets than for Gliese 710's whereas Gliese 710's comets' inclination, eccentricity, and energy proxy have higher spreads. This means that the Sun's comets experience a greater net change in perihelion, aphelion, and semi-major axis than Gliese 710's comets and a smaller change in inclination, eccentricity, and energy. This increase in orbital parameters in known as "dynamical heating".

Figure 13 shows the semi-major axis vs eccentricity distributions of the Sun's and Gliese 710's comets at the beginning and end of the simulation. The comets that reach the highest semi-major axes also have the highest eccentricities: 11 out of 12 of the Suns comets reaching semi-major axes higher than 1.5×10^5 AU had eccentricities over 0.9. This corroborates our earlier finding of the aphelion being much easier to shift than the perihelion and that the way this is done is by increasing the eccentricity. The reason that there are no new comets with semi-major axes of $\sim 2 \times 10^5$ AU at low eccentricities is because to achieve such high semi-major axes without also increasing the eccentricity would be to raise the perihelion. Figure 13 also shows a leakage of the hard border of 10^5 AU we imposed in the simulation. This indicates that it is possible for comets to be further out that 10^5 AU and remain part of the Oort cloud. A different distribution in which the distribution of semi-major axis is dependant not only on a factor γ but also on eccentricity might be more accurate. The $e(a)$ relation would probably be exponential in nature for comets beyond the "boundary" of the

Oort cloud, judging by the plots in Figure 13. Of course, this simulation does not take into account the gravity of other nearby stars and the galactic tide so making inferences about the structure of the outer edge of the Oort cloud could be dangerous. Several of the comets going beyond 10^5 AU would likely be lost from the Oort cloud.

Figure 13 also shows that Gliese 710's comets are more easily lifted to further orbits. 0.59% of Gliese 710's comets achieved semi-major axes greater than the initial limit to the semi-major axis, where as only 0.21% of the Sun's comets did the same. This is agrees with the earlier result of a higher percentage of Gliese 710's comets which became unbound: 0.051% as opposed to the Sun's 0.019%.

Figures 14 and 15 show the eccentricities and semi-major axes of the comets before and after the encounter plotted against each other. No significant correlation between the values of e and a before the encounter and the values of e and a after the encounter for comets that reach extreme values of e and a can be see. This implies that comets of any eccentricity are equally likely to reach extreme eccentricities of $e > 1$. This does not fit well with our result of 71% which became unbound were in the upper half of the initial energy distribution and the positive correlation seen between the comets that reach positive energies after the encounter and initial energy, as seen in Figure 16. This implies that eccentricity does not correlate significantly with a comet's energy.

4.5 Velocities of unbound comets

Figure 17 shows the velocity distribution of the comets which became unbound from their host stars. The velocities of these comets range from $\sim$ 0.03 AU/yr to $\sim$ 0.17 AU/yr relative to their host stars. These velocities are small compared to the velocities of other stars relative to our Sun. Gliese 710, for example, presently has a radial velocity of -3.0 AU/yr relative to the sun and the velocity of the Sun relative to the local standard of rest is 3.8 AU/yr according to Schönrich et al. (2010b).

This means that the unbound comets are not dynamically distinct from the Sun and that interstellar comets we encounter will likely have peculiar velocities similar to their star system of origin.

4.6 Other limitations

A limitation of this study is that the galactic tide has not been taken into account. Rickman et al. (2008) found a synergistic effect between the galactic tide and stellar encounters on the number of comets injected into the inner solar system. This means that the percentage of comets injected into the inner solar system will in reality be higher.

5 Conclusion

We used an N-body simulator named `REBOUND` to run two simulations of duration 4 Myr and 80,000 yr respectively. In both, we simulated the future encounter between the Sun and Gliese 710 in which both stars had a comet cloud.

The Sun's and Gliese 710's comet clouds are affected in various ways. Gliese 710, for example, loses a higher percentage of comets despite its comets being equally bound to its star as that was the selection criterion for the size of Gliese 710's comet cloud (see §2.2, page 14). In this simulation, Gliese 710's comets also experience greater changes in inclination, eccentricity, and energy while experiencing a lesser change in perihelion, aphelion, and semi-major axis than the Sun's comets. This is evidenced in Figure 9 and the FWHM of the distributions of these changes can be seen in Table 3.

A small percentage of between 0.019% and 0.117% of the Oort cloud's[8] comets are lost in this encounter, depending on how many of the comets entering the planetary region are removed from the Oort cloud − either becoming unbound or tightly bound to the inner solar system due to interactions with the planets. Using approximations of this loss and a rate of encounters of 0.23 per Myr within 10^5 AU (Bailer-Jones et al., 2018) gives a percentage loss of $\sim$ 4.3% - 20% per Gyr from encounters like this one. Our result stands in contrast to the loss rate of 2.4% derived by Hanse et al. (2018). The assumption we made when calculating these 4.3% - 20% figures was that this encounter with Gliese 710's was an approximate proxy for the 2.5 other expected number of encounters to take place within 10^5 AU in the next 15 Myr found by Bailer-Jones et al. (2018). The discrepancy between our values of 4.3% - 20% and Hanse et al. (2018)'s value of 2.4% thus speaks to how bad of an assumption this was and thus how comparatively rare an encounter like Gliese 710's is. In addition to this, our minimum encounter distance being 19.2% smaller than the literature value (De la Fuente Marcos and De la Fuente Marcos, 2018) also inflated our rate of comet loss as well. It also suggests that most comets which enter the planetary region return to the Oort cloud, as this was the assumption made when calculating the lower bound.

Figures 6 and 7 show no significant change in the large scale structure of either comet cloud in the simulations: there is no visible change in the r-distribution of either comet cloud pre- and post-encounter in Figure 7 and this is reflected in the stable mean and median r-values plotted over time in 6. However, Figure 12 shows a slight bias towards an increase in the semi-major axis and aphelion around the time of minimum distance. The peaks of these lines correspond to PBP values of 1.7% and 0.75% more median change in the positive direction at the time of minimum distance of the semi-major axis and aphelion respectively for the Oort cloud in Simulation 2. The PBP of the perihelion for the Oort cloud was only 0.075%, where as the PBP of the eccentricity was 0.14%. These numbers together show that the preference for the change in orbital parameters upon perturbation from an encounter like Gliese 710's is for the orbits to experience an increase the semi-major axis, aphelion, and eccentricity while the perihelion is essentially held constant.

The main effect found on the Oort cloud's structure was a slight net increase in the semi-

[8] "The Oort cloud" refers to the Sun's comet cloud, as outlined in the introduction.

major axes (1.7%) and aphelia (0.75%) of the comets' orbits around the time of minimum distance with a corresponding slight increase of 0.14% in eccentricity for the Sun's comets. The distribution of changes can be seen in Figure 9 and their FWHM can be seen in Table 3. Several of the Oort cloud's comets (0.21%) also reached semi-major axis over the 10^5 AU limit of the initial conditions, as can be seen in Figure 10 and 13. The ones which reached the highest semi-major axes of 2×10^5 (11 out of 12) had resulting eccentricities between 0.9 and 1.

The biggest effect seen has been the Oort cloud's 0.019% - 0.117% loss of comets and Gliese 710's comet cloud's 0.051% - 0.172% loss of comets. 50 of the 70 comets (71%) which became unbound were in the upper half of the initial energy ($-1/a$) distribution. Of the 219 comets that were injected into the planetary regions, 147 (67%) were in the lower half of the energy distribution. The unbound comets have velocities relative to their host star ranging between 0.03 AU/yr and 0.17 AU/yr, which are very low velocities relative to the motion of local stars. Gliese 710 and the Sun currently have a relative radial velocity of -3.0 AU/yr, the velocity of the Sun relative the the local standard of rest is 3.8 AU/yr and voyager 1 is currently travelling away from the solar system at 3.6 AU/yr.

Acknowledgements

I would like to thank my thesis supervisors Kateryna Frantseva and Nickolas Oberg for their invaluable input, guidance, and patience in both my research and the writing of this paper.

This work has made use of data from the European Space Agency (ESA) mission *Gaia* (`https://www.cosmos.esa.int/gaia`), processed by the *Gaia* Data Processing and Analysis Consortium (DPAC, `https://www.cosmos.esa.int/web/gaia/dpac/consortium`).

Funding for the DPAC has been provided by national institutions, in particular the institutions participating in the *Gaia* Multilateral Agreement.

The simulations in this paper made use of the REBOUND code which can be downloaded freely at `http://github.com/hannorein/rebound`.

References

K. Altwegg, H. Balsiger, A. Bar-Nun, J. J. Berthelier, A. Bieler, P. Bochsler, C. Briois, U. Calmonte, M. Combi, J. De Keyser, P. Eberhardt, B. Fiethe, S. Fuselier, S. Gasc, T. I. Gombosi, K. Hansen, M. Hässig, A. Jäckel, E. Kopp, A. Korth, L. LeRoy, U. Mall, B. Marty, O. Mousis, E. Neefs, T. Owen, H. Rème, M. Rubin, T. Sémon, C.-Y. Tzou, H. Waite, and P. Wurz. 67p/churyumov-gerasimenko, a jupiter family comet with a high d/h ratio. *Science*, 347(6220), 2015. ISSN 0036-8075. doi: 10.1126/science.1261952. URL `https://science.sciencemag.org/content/347/6220/1261952`.

M. F. A'Hearn. *Cometary Science: The Present and Future*, page 17. 2004.

C. A. L. Bailer-Jones, J. Rybizki, R. Andrae, and M. Fouesneau. New stellar encounters discovered in the second Gaia data release. A&A, 616:A37, Aug 2018. doi: 10.1051/0004-6361/201833456.

M. Bennett and J. Bovy. Vertical waves in the solar neighbourhood in Gaia DR2. MNRAS, 482(1):1417–1425, Jan 2019. doi: 10.1093/mnras/sty2813.

H. Beust, A. M. Lagrange-Henri, A. V. Madjar, and R. Ferlet. The Beta Pictoris circumstellar disk. X - Numerical simulations of infalling evaporating bodies. A&A, 236:202–216, Sept. 1990.

J. Bovy. galpy: A python Library for Galactic Dynamics. ApJS, 216:29, Feb. 2015. doi: 10.1088/0067-0049/216/2/29.

J. Chambers. Why halley-types resonate but long-period comets don't: A dynamical distinction between short- and long-period comets. *Icarus*, 125(1):32 – 38, 1997. ISSN 0019-1035. doi: https://doi.org/10.1006/icar.1996.5567. URL `http://www.sciencedirect.com/science/article/pii/S0019103596955670`.

R. De la Fuente Marcos and C. De la Fuente Marcos. An Independent Confirmation of the Future Flyby of Gliese 710 to the Solar System Using Gaia DR2. *Research Notes of the American Astronomical Society*, 2(2):30, May 2018. doi: 10.3847/2515-5172/aac2d0.

L. Dones, P. R. Weissman, H. F. Levison, and M. J. Duncan. *Oort cloud formation and dynamics*, page 153. 2004.

M. Duncan, T. Quinn, and S. Tremaine. The Formation and Extent of the Solar System Comet Cloud. In *Bulletin of the American Astronomical Society*, volume 19 of BAAS, page 742, Mar. 1987.

P. D. Feldman, M. F. A'Hearn, J.-L. Bertaux, L. M. Feaga, J. W. Parker, E. Schindhelm, A. J. Steffl, S. A. Stern, H. A. Weaver, and H. Sierks. Measurements of the near-nucleus coma of comet 67P/Churyumov-Gerasimenko with the Alice far-ultraviolet spectrograph on Rosetta. A&A, 583:A8, Nov 2015. doi: 10.1051/0004-6361/201525925.

F. Feng and C. A. L. Bailer-Jones. Finding the imprints of stellar encounters in long-period comets. MNRAS, 454:3267–3276, Dec. 2015. doi: 10.1093/mnras/stv2222.

M. C. Festou, H. U. Keller, and H. A. Weaver. *A brief conceptual history of cometary science*, page 3. 2004.

Gaia Collaboration, T. Prusti, J. H. J. de Bruijne, A. G. A. Brown, A. Vallenari, C. Babusiaux, C. A. L. Bailer-Jones, U. Bastian, M. Biermann, D. W. Evans, and et al. The Gaia mission. A&A, 595:A1, Nov. 2016. doi: 10.1051/0004-6361/201629272.

Gaia Collaboration, A. G. A. Brown, A. Vallenari, T. Prusti, J. H. J. de Bruijne, C. Babusiaux, C. A. L. Bailer-Jones, M. Biermann, D. W. Evans, L. Eyer, and et al. Gaia Data Release 2. Summary of the contents and survey properties. A&A, 616:A1, Aug. 2018. doi: 10.1051/0004-6361/201833051.

J. García-Sánchez, R. A. Preston, D. L. Jones, P. R. Weissman, J.-F. Lestrade, D. W. Latham, and R. P. Stefanik. Stellar encounters with the oort cloud based on [ITAL]hipparcos[/ITAL] data. *The Astronomical Journal*, 117(2):1042–1055, feb 1999. doi: 10.1086/300723. URL `https://doi.org/10.1086%2F300723`.

Gravity Collaboration, R. Abuter, A. Amorim, N. Anugu, M. Bauböck, M. Benisty, J. P. Berger, N. Blind, H. Bonnet, W. Brandner, A. Buron, C. Collin, F. Chapron, Y. Clénet, V. Coudé Du Foresto, P. T. de Zeeuw, C. Deen, F. Delplancke-Ströbele, R. Dembet, J. Dexter, G. Duvert, A. Eckart, F. Eisenhauer, G. Finger, N. M. Förster Schreiber, P. Fédou, P. Garcia, R. Garcia Lopez, F. Gao, E. Gendron, R. Genzel, S. Gillessen, P. Gordo, M. Habibi, X. Haubois, M. Haug, F. Haußmann, T. Henning, S. Hippler, M. Horrobin, Z. Hubert, N. Hubin, A. Jimenez Rosales, L. Jochum, K. Jocou, A. Kaufer, S. Kellner, S. Kendrew, P. Kervella, Y. Kok, M. Kulas, S. Lacour, V. Lapeyrère, B. Lazareff, J. B. Le Bouquin, P. Léna, M. Lippa, R. Lenzen, A. Mérand, E. Müler, U. Neumann, T. Ott, L. Palanca, T. Paumard, L. Pasquini, K. Perraut, G. Perrin, O. Pfuhl, P. M. Plewa, S. Rabien, A. Ramírez, J. Ramos, C. Rau, G. Rodríguez-Coira, R. R. Rohloff, G. Rousset, J. Sanchez-Bermudez, S. Scheithauer, M. Schöller, N. Schuler, J. Spyromilio, O. Straub, C. Straubmeier, E. Sturm, L. J. Tacconi, K. R. W. Tristram, F. Vincent, S. von Fellenberg, I. Wank, I. Waisberg, F. Widmann, E. Wieprecht, M. Wiest, E. Wiezorrek, J. Woillez, S. Yazici, D. Ziegler, and G. Zins. Detection of the gravitational redshift in the orbit of the star S2 near the Galactic centre massive black hole. A&A, 615:L15, Jul 2018. doi: 10.1051/0004-6361/201833718.

R. O. Gray, C. J. Corbally, R. F. Garrison, M. T. McFadden, E. J. Bubar, C. E. McGahee, A. A. O'Donoghue, and E. R. Knox. Contributions to the Nearby Stars (NStars) Project: Spectroscopy of Stars Earlier than M0 within 40 pc-The Southern Sample. AJ, 132(1): 161–170, Jul 2006. doi: 10.1086/504637.

J. Hanse, L. Jílková, S. F. Portegies Zwart, and F. I. Pelupessy. Capture of exocomets and the erosion of the Oort cloud due to stellar encounters in the Galaxy. MNRAS, 473(4): 5432–5445, Feb 2018. doi: 10.1093/mnras/stx2721.

A. Higuchi and E. Kokubo. Effect of Stellar Encounters on Comet Cloud Formation. AJ, 150(1):26, Jul 2015. doi: 10.1088/0004-6256/150/1/26.

H. F. Levison, L. Dones, and M. J. Duncan. The origin of halley-type comets: Probing the inner oort cloud. *The Astronomical Journal*, 121(4):2253–2267, apr 2001. doi: 10.1086/319943. URL `https://doi.org/10.1086%2F319943`.

L. Lindegren, J. Hernández, A. Bombrun, S. Klioner, U. Bastian, M. Ramos-Lerate, A. de Torres, H. Steidelmüller, C. Stephenson, D. Hobbs, U. Lammers, M. Biermann, R. Geyer, T. Hilger, D. Michalik, U. Stampa, P. J. McMillan, J. Castañeda, M. Clotet, G. Comoretto, M. Davidson, C. Fabricius, G. Gracia, N. C. Hambly, A. Hutton, A. Mora, J. Portell, F. van Leeuwen, U. Abbas, A. Abreu, M. Altmann, A. Andrei, E. Anglada, L. Balaguer-Núñez, C. Barache, U. Becciani, S. Bertone, L. Bianchi, S. Bouquillon, G. Bourda, T. Brüsemeister, B. Bucciarelli, D. Busonero, R. Buzzi, R. Cancelliere, T. Carlucci, P. Charlot, N. Cheek, M. Crosta, C. Crowley, J. de Bruijne, F. de Felice, R. Drimmel, P. Esquej, A. Fienga, E. Fraile, M. Gai, N. Garralda, J. J. González-Vidal, R. Guerra, M. Hauser, W. Hofmann, B. Holl, S. Jordan, M. G. Lattanzi, H. Lenhardt, S. Liao, E. Licata, T. Lister, W. Löffler, J. Marchant, J.-M. Martin-Fleitas, R. Messineo, F. Mignard, R. Morbidelli, E. Poggio, A. Riva, N. Rowell, E. Salguero, M. Sarasso, E. Sciacca, H. Siddiqui, R. L. Smart, A. Spagna, I. Steele, F. Taris, J. Torra, A. van Elteren, W. van Reeven, and A. Vecchiato. Gaia Data Release 2. The astrometric solution. A&A, 616:A2, Aug. 2018. doi: 10.1051/0004-6361/201832727.

E. E. Mamajek, S. A. Barenfeld, V. D. Ivanov, A. Y. Kniazev, P. Väisänen, Y. Beletsky, and H. M. J. Boffin. The Closest Known Flyby of a Star to the Solar System. ApJ, 800 (1):L17, Feb 2015. doi: 10.1088/2041-8205/800/1/L17.

J. H. Oort. The structure of the cloud of comets surrounding the Solar System and a hypothesis concerning its origin. Bull. Astron. Inst. Netherlands, 11:91–110, Jan. 1950.

H. Rein and S.-F. Liu. REBOUND: an open-source multi-purpose N-body code for collisional dynamics. A&A, 537:A128, Jan. 2012. doi: 10.1051/0004-6361/201118085.

H. Rickman, M. Fouchard, G. B. Valsecchi, and C. Froeschlé. Algorithms for Stellar Perturbation Computations on Oort Cloud Comets. *Earth Moon and Planets*, 97:411–434, Dec. 2005. doi: 10.1007/s11038-006-9113-7.

H. Rickman, M. Fouchard, C. Froeschlé, and G. B. Valsecchi. Injection of Oort Cloud comets: the fundamental role of stellar perturbations. *Celestial Mechanics and Dynamical Astronomy*, 102:111–132, Sept. 2008. doi: 10.1007/s10569-008-9140-y.

R. Schönrich, J. Binney, and W. Dehnen. Local kinematics and the local standard of rest. MNRAS, 403:1829–1833, Apr. 2010a. doi: 10.1111/j.1365-2966.2010.16253.x.

R. Schönrich, J. Binney, and W. Dehnen. Local kinematics and the local standard of rest. MNRAS, 403(4):1829–1833, Apr 2010b. doi: 10.1111/j.1365-2966.2010.16253.x.